AUTHOR QUERY FORM

ELSEVIER	Journal: YQRES Article Number: 3684	Please e-mail your responses and any corrections to: E-mail: Corrections.ESSD@elsevier.spitech.com

Dear Author,

Please check your proof carefully and mark all corrections at the appropriate place in the proof (e.g., by using on-screen annotation in the PDF file) or compile them in a separate list. Note: if you opt to annotate the file with software other than Adobe Reader then please also highlight the appropriate place in the PDF file. To ensure fast publication of your paper please return your corrections within 48 hours.

For correction or revision of any artwork, please consult http://www.elsevier.com/artworkinstructions.

We were unable to process your file(s) fully electronically and have proceeded by

☐ Scanning (parts of) your article ☐ Rekeying (parts of) your article ☐ Scanning the artwork

Any queries or remarks that have arisen during the processing of your manuscript are listed below and highlighted by flags in the proof. Click on the 'Q' link to go to the location in the proof.

Location in article	Query / Remark: click on the Q link to go Please insert your reply or correction at the corresponding line in the proof
Q1	Your article is registered as a regular item and is being processed for inclusion in a regular issue of the journal. If this is NOT correct and your article belongs to a Special Issue/Collection please contact rhosan.sotomayor@elsevier.com immediately prior to returning your corrections.
Q2	The author names have been tagged as given names and surnames (surnames are highlighted in pink color). Please confirm if they have been identified correctly.
Q3, Q5	This sentence has been slightly modified for clarity. Please check and confirm if the meaning is still correct.
Q4	The citation "Vepraskas, 2001" has been changed to match the author name/date in the reference list. Please check here and correct if necessary.
Q6	Uncited references: This section comprises references that occur in the reference list but not in the body of the text. Please position each reference in the text or, alternatively, delete it. Thank you. Please check this box if you have no corrections to make to the PDF file. ☐

Thank you for your assistance.

Supplementary Table 1 GPS coordinates for locations of paleosol sites and locations of 6 Chapati Tuff samples used for parent material in mass-balance calculations.

Supplementary Table 2 Estimated soil characterization for PTK A site paleosol using Vertisol pedotransfer functions of Nordt and Driese (2010a).

Supplementary Table 3 Estimated soil characterization data for E4 site paleosol using Vertisol pedotransfer functions of Nordt and Driese (2010a).

Supplementary Fig. 1 Mass-balance geochemistry of Level 22 Zinj archaeological site paleosols (important trends are summarized in Table 1), normalized to composition of model Chapati Tuff parent material at each site, and assuming immobile TiO_2 during weathering. (A–D) Comparison of translocations for Ba, Sr, Rb, and P_2O_5 (feldspar weathering and biocycling cations): note that PTK A and PTK B both show 25–175% net gain in P_2O_5 and erratic depth patterns of both losses and gains in Ba, Sr and Rb; E4 and FLK both show up to 100% net gains in Rb, and general 25–50% net losses in Ba, Sr, and P_2O_5, except for a 10–25% net gain in Ba and Sr in the upper 15 cm of E4. (E–H) Comparison of translocations for Cu, Ni, Pb, and Zn (plant microelements and elements sorbed to organic C): note that depth patterns for PTK A and PTK B are somewhat similar, with PTK A showing 25–75% net losses of Pb and Z at the surface, and net gains of 25–150% of Cu and Ni at depths of 5–33 cm; in contrast, PTK B has 25–50% losses of Pb and Zn, and 50–125% net gains of Cu and Ni; E4 shows up to 200% net gains of Cu and Ni, 25% net gain of Zn, and 5–50% net loss of Pb; FLK calculations indicate 25–100% additions of Cu and Ni, 5–60% net losses of Pb and Zn, but with 5–50% net gain of Zn from 10–33 cm depth. (I–L) Comparison of translocations for La, Li, Th, and Y (Lanthanide and immobile elements): note that depth patterns for PTK A and PTK B are somewhat similar, with PTK A showing 25–75% net losses of all 4 elements at the surface, and net gains of 5–25% depths of 10–33 cm; in contrast, PTK B has 25–50% losses of La and Li, and 25–50% net gains of Th and Y; E4 shows up to 300% net gains of Li, 25–100% net gains of La, Th, and Y; FLK calculations indicate up to 325% additions of Li, 5–60 losses of La, Th, and Y, but with 5–50% net gains of La and Th from 15–33 cm depth.

Supplementary Fig. 2 Estimates of soil characterization data of Level 22 Zinj archaeological site paleosols with vertic (Vertisol-like) properties versus depth, using pedotransfer functions of Nordt and Driese (2010a). For full characterization of FLK paleosol profile, see Tables 2 and 3, and for full characterization of PTK A and E4 paleosol sites, see Supplementary Tables 2 and 3. (A) Estimated pH (water) showing overall lower estimated pH for paleosol at PTK A compared with FLK and E4; all soil pH estimates are quite high and suggest an alkaline soil environment. (B) Estimated $CaCO_3$ (%) showing overall higher estimated $CaCO_3$% for paleosol at PTK A compared with FLK and E4, which may reflect proximity to spring tufa system. (C) Estimated organic C (%) using Pb pedotransfer function, presented in Nordt et al. (2012), showing higher organic C in surface part of paleosol at PTK A, as well as overall high organic C contents. (D) Estimated Fe_d (%) showing overall higher pedogenic Fe in PTK A paleosol compared with paleosols at FLK and E4, perhaps reflecting greater intensity of weathering of Fe-bearing minerals. (E) Estimated ESP (%) showing overall slightly higher ESP for paleosol at PTK A site, however, all estimated ESP values at all sites are quite high, and collectively suggest some possible limitations on plant communities due to accumulation of salts. (F) Sum of all exchangeable bases (Σ ex. Ca^{2+} + ex. Mg^{2+} + ex. Na^{+} + ex. K^{+}, in cmoles charge per kg of soil) showing exceptionally high base accumulations, largely due to Ca and Mg in smectites), with highest values estimated for paleosol at PTK A site.

Appendix 1 Bulk geochemistry of Zinj clay paleosol and Chapati Tuff.

Quaternary Research xxx (2015) xxx–xxx

Contents lists available at ScienceDirect

Quaternary Research

journal homepage: www.elsevier.com/locate/yqres

Paleoenvironmental reconstruction of a paleosol catena, the Zinj archeological level, Olduvai Gorge, Tanzania

Steven G. Driese[a,*], Gail M. Ashley[b]

[a] Terrestrial Paleoclimatology Research Group, Department of Geology, One Bear Place #97354, Baylor University, Waco, TX 76798-7354 USA
[b] Department of Earth & Planetary Sciences, Rutgers University, Piscataway, NJ 08854-8066, USA

ARTICLE INFO

Article history:
Received 5 June 2015
Available online xxxx

Keywords:
Paleosol catena
Early Pleistocene
Zinj archeological level
Olduvai Gorge
Tanzania

ABSTRACT

Paleosols record paleoclimatic processes in the Earth's Critical Zone and are archives of ancient landscapes associated with archeological sites. Detailed field, micromorphologic, and bulk geochemical analysis of paleosols were conducted near four sites at Olduvai Gorge, Tanzania within the same stratigraphic horizon as the *Zinjanthropus* (*Paranthropus*) *boisei* archeological site. Paleosols are thin (<35 cm), smectitic, and exhibit Vertisol shrink–swell features. Traced across the paleolandscape over 1 km and just beneath Tuff IC (1.845 Ma), the paleosols record a *paleocatena* in which soil moisture at the four sites was supplemented by seepage additions from adjacent springs, and soil development was enhanced by this additional moisture. Field evidence revealed an abrupt lateral transition in paleosol composition at the PTK site (<1.5 m apart) in which paleosol B, formed nearest the spring system, is highly siliceous, vs. paleosol A, formed in smectitic clay. Thin-section investigations combined with mass-balance geochemistry, using Chapati Tuff as parent material and assuming immobile Ti, show moderately intense weathering. Pedotransfer functions indicate a fertile soil system, but sodicity may have limited some plant growth. Paleosol bulk geochemical proxies used to estimate paleoprecipitation (733–944 mm/yr), are higher than published estimates of 250–700 mm/yr using δD values of lipid biomarkers.

Introduction

Paleosols are increasingly recognized for their utility in paleoclimate and paleolandscape reconstructions, as well as for reconstructions of paleoatmospheric chemistry (Kraus, 1999; Retallack, 2001; Sheldon and Tabor, 2009; Driese and Nordt, 2013). Increasingly paleosols are interpreted as "paleo-Critical Zones" (Nordt and Driese, 2013; Ashley et al., 2014a) which have potential for not only reconstructing more than paleoclimate, but also biogeochemical cycling and ecosystem function (Nordt and Driese, 2010a; Nordt et al., 2012). Ashley et al. (2014a) summarized the paleosol diversity in the Olduvai Basin, Tanzania, as consisting primarily of fluvial plain paleo-Aridisols, lake clay paleo-Vertisols, and volcaniclastic (pyroclastic fan) paleo-Andisols, with the development of soils strongly influenced by proximity to freshwater springs and wetlands. Availability of this supplemental water in what has been reconstructed to be an overall arid to semi-arid paleolandscape greatly affected plant ecosystems and early human habitats (Magill et al., 2013a,b; Cuthbert and Ashley, 2014).

Olduvai Gorge, a river incision sliced through the sedimentary record of the Olduvai basin, became world famous with the discovery of a hominin fossil *Zinjanthropus boisei* in 1959 by Mary and Louis Leakey (Leakey, 1959). The fossil was found to be part of a very dense concentration of vertebrate fossils, stone tools and remains of another hominin, *Homo habilis*. The site (FLK, named in 1959 by Louis Leakey for **F**rida **L**eakey **K**orongo, his first wife) is in an archeological horizon called Level 22. Since 1959 there have been a wide range of studies focused on various aspects of the FLK site: the physical anthropology of the hominin "Zinj" (Tobias, 1967), the typology of stone tools (Potts, 1988), taphonomy of the bones (Bunn and Kroll, 1986; Oliver, 1994; Domínguez-Rodrigo et al., 2007, 2010a,b), general ecology of the site (Plummer and Bishop, 1994; Sikes, 1994; Ashley et al., 2010a), and even speculation on the hominin diet (van der Merwe et al., 2008), but the research community has completely overlooked the paleosol in which the artifacts were archived and essentially nothing is known about the paleosol itself. As a paleo-Critical Zone, Level 22 holds important information about this time and place when early humans were using the landscape.

Objectives

The primary objectives for this study are: (1) to interpret the paleopedology and paleoenvironments (MAP, seasonality), based on paleosol morphology, micromorphology, and geochemistry of the 0.35 m thick, paleosol at archeological Level 22 beneath Tuff IC, at the FLK site in Olduvai Gorge, Tanzania, and related correlative sites at PTK A, PTK B and E4, and (2) to interpret the relationships between paleosol development, fault-controlled spring hydrology, and overall paleo

* Corresponding author.
E-mail address: Steven_Driese@baylor.edu (S.G. Driese).

http://dx.doi.org/10.1016/j.yqres.2015.10.007
0033-5894/© 2015 Published by Elsevier Inc. on behalf of University of Washington.

Lake Olduvai basin evolution, and thus better constrain the paleoenvironmental context for early hominins.

Background

Geological setting

Olduvai Gorge is located in a shallow sedimentary basin on the margin of the East African Rift System in northern Tanzania (Fig. 1). The basin has a 2.2 Ma-long record composed of intercalated volcaniclastics, volcanic lavas and tuffs, and minor carbonates. It is world famous for its rich paleontological and cultural records (Leakey, 1971; Hay, 1976). The Gorge resulted from river incision during the late Pleistocene that was triggered by rift-related tectonics (Hay, 1976), and provides exposures of deposits recording a saline lake, fluctuating lake-margin, freshwater spring (proximal to faults), fluvial plain (northwest) and pyroclastic alluvial fan (southeast) paleoenvironments (Fig. 1).

The field study site is located within a 0.5-km^2 area at the "junction", the confluence of Main and Side Gorges in the Olduvai Basin (Figs. 1, 2; Supplementary Table 1). The sediments are clays and silts deposited on a broad flat lake margin of paleo Lake Olduvai, a playa that fluctuated under both long-term (Milankovitch) precession climate cycles (Ashley, 2007; Magill et al., 2013a,b) and shorter term (annual) cycles (Liutkus et al., 2005). Fine sediment was deposited during lake flooding that was later subject to pedogenesis during subaerial exposure. Uribelarrea et al. (2014) reconstructed the paleolandscape at 1.84 Ma for a radius of circa 1000 m from the FLK Zinj site using descriptions of the Level 22 physical stratigraphy at 30 sites and applying a correction for tectonic tilt associated with nearby faults. The stratigraphy has been well-dated with paleomagnetic polarity (Fig. 3) and single-crystal argon dating of marker tuffs that can be traced though the basin (Deino, 2012) and divided into 5 major stratigraphic units (Hay, 1976).

The time-slice target for this study is within middle Bed I directly beneath Tuff IC. Tuff IC geochemistry is summarized in McHenry (2004, 2005) and McHenry et al. (2008). Uribelarrea et al. (2014, their Fig. 2) defined a schematic circa 2.5-m-thick type section for strata occurring between basalt basement and Tuff IC. Their "Zinj clay" interval lying beneath Tuff IC is equivalent to the Zinj paleosol of our study; importantly, Uribelarrea et al. (2014, their Fig. 2) defined a new stratigraphic unit termed "the Chapati Tuff" that occurs immediately beneath the Zinj clay (paleosol), and which is probably the parent material for the paleosol. The bulk chemistry and mineralogy of the saline–alkaline lacustrine waxy clays and related earthy clay deposits of lowermost Bed II were characterized previously by Deocampo et al. (2002) and Liutkus and Ashley, 2003, with additional studies by Hover and Ashley (2003) and Deocampo et al. (2009) focusing on clay chemistry and diagenesis.

Archeology

Level 22 was defined by Mary Leakey during excavations at FLK in 1960–1961 (Leakey, 1971) and *Paranthropus boisei* the oldest hominin fossil at that time (originally called *Z. boisei*) was discovered there. The excavation of a 315-m^2 area in Level 22 directly under Tuff IC yielded ~2500 Oldowan stone artifacts and 3500 fossil bone specimens including remains of *H. habilis*. This localized, high-density co-occurrence of Oldowan tools and fossilized bones is the FLK archeological site, the location of which has been linked to a spring and wetland 200 m to the north (Domínguez-Rodrigo et al., 2007; Ashley et al., 2010a,b,c). Two additional, localized high-density sites (e.g., dozens of bones per square meter) were recently discovered in Level 22: PTK (**P**hillip **T**obias **K**orongo) is 320 m south of FLK, while AMK (**A**min **M**turi **K**orongo) is ~360 m southeast of FLK (Fig. 2). Both sites are currently being excavated and interpreted. An early announcement of hominin fossils (hand bones) found at PTK was made this year (Domínguez-Rodrigo et al., 2015).

Methods

During the summers of 2008, 2013 and 2014, Level 22 strata were located with GPS, measured and described at the four sites (Figs. 1, 2;

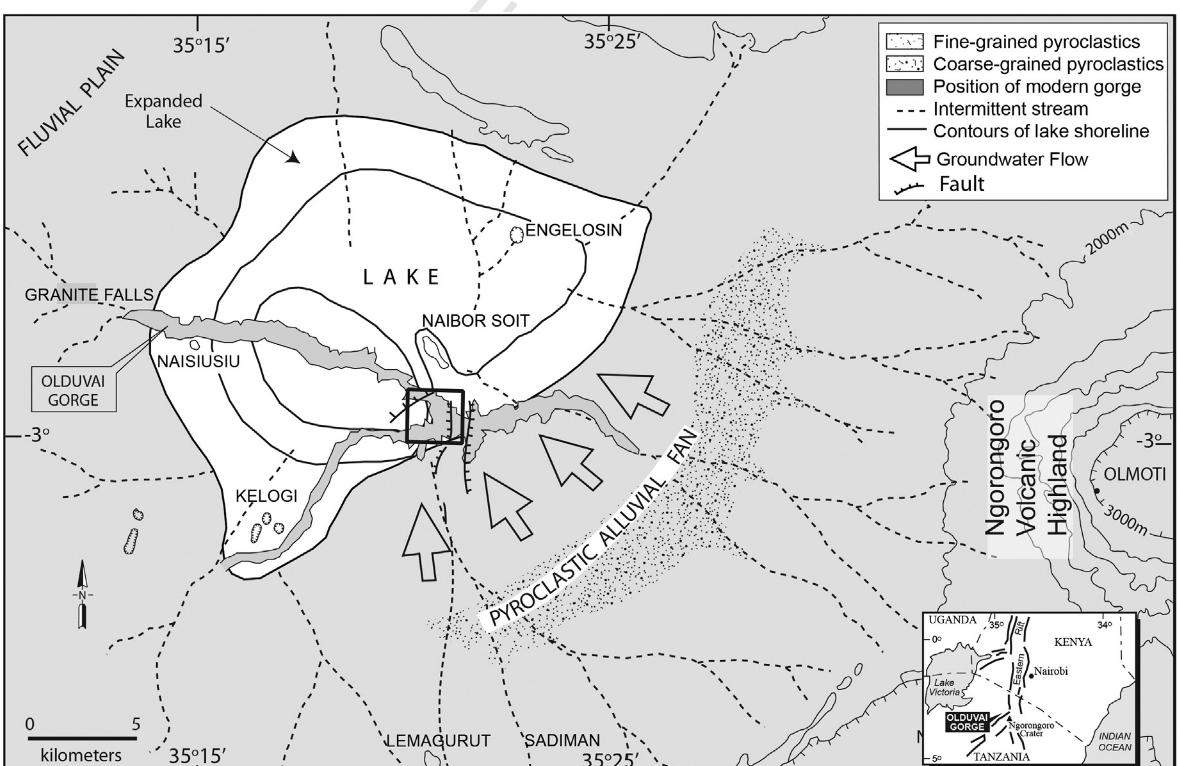

Fig. 1. Location map of Level 22 paleosol catena at the FLK-Zinj archeological site, Olduvai Gorge, Tanzania (modified from Ashley et al., 2010a).

Please cite this article as: Driese, S.G., Ashley, G.M., Paleoenvironmental reconstruction of a paleosol catena, the Zinj archeological level, Olduvai Gorge, Tanzania, Quaternary Research (2015), http://dx.doi.org/10.1016/j.yqres.2015.10.007

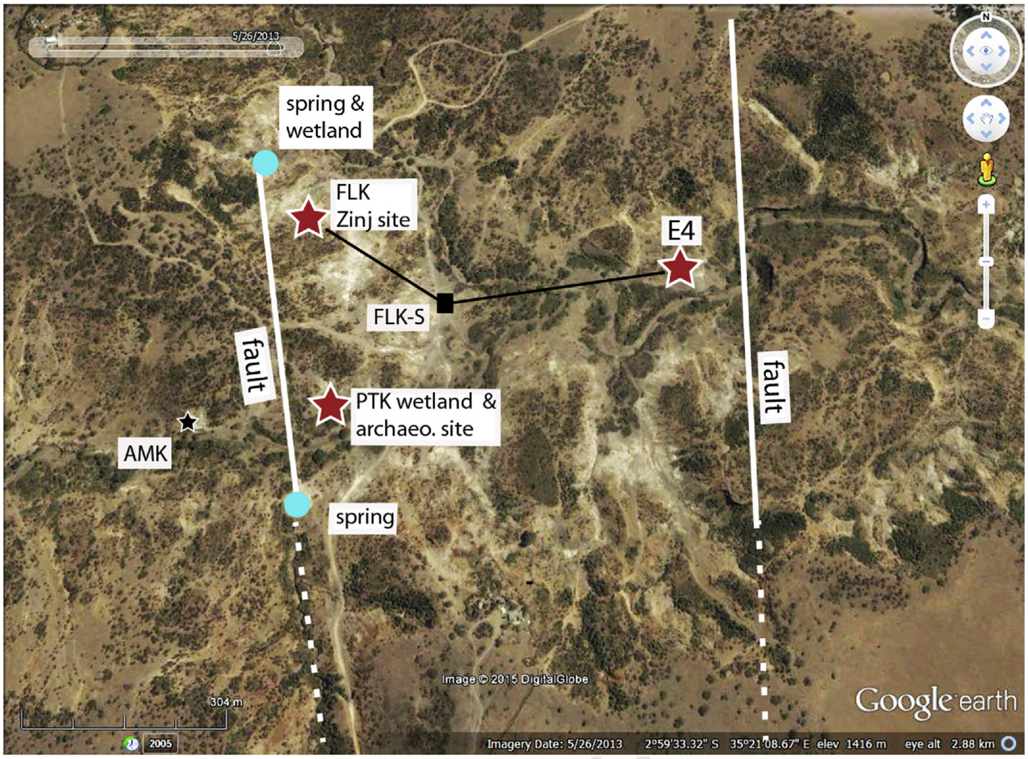

Fig. 2. Google Earth® modern surface map of portion of Olduvai Gorge, Tanzania, showing locations of paleosol sampling sites (FLK Zinj, PTK A and B, and E4 site), stratigraphic section FLK-S, location of transect shown in Fig. 4, mapped faults, and previously identified paleo-spring deposits. Note close association of two archeological sites (FLK and PTK A and PTK B) with springs, which would have served as a source of potable water for both animals and hominins.

Supplementary Table 1) in detail using standard field methods. Samples were classified as either waxy clay, earthy clay, or reworked tuff based on field properties, as well as geochemical and mineralogical properties defined by Hay (1976), Ashley and Driese (2000) and Deocampo et al. (2002). Samples weighing approximately 500 g were collected every 3–5 cm in a vertical 10-cm-wide section that extended 35 cm below Tuff IC. In addition, blocks of sediment were collected for thin sections. Fig. 4 shows the PTK A and B paleosol profiles located beneath Tuff IC; the other sites were sampled similarly. The four sections were correlated based on their position directly underlying Tuff IC, an airfall tuff. In the course of the study paleosols were measured and described in further detail using descriptive properties for paleosols and soils outlined in Retallack (1988) and Schoeneberger et al. (2012), respectively. Six bulk samples of Chapati Tuff were collected as representative of paleosol parent material (Supplementary Table 1).

Laboratory

Paleosols were sampled for both oriented and unoriented thin-section samples, which were subsequently prepared by a commercial lab (Spectrum Petrographics, Inc.) as either 1 × 2 cm (7 samples) or 5 × 7 cm thin-sections (3 samples). After initial scanning and digitization on a flat-bed at 600 dpi, the thin sections were examined at Baylor University using an Olympus BX51 Research microscope equipped with standard plane-polarized (PPL) and crossed-polarized (XPL) light, as well as with UV fluorescence (UVf), and each uncovered slide surveyed freely for stand-out features of interest, and then photographed using a 7.6 Mpx Leica® digital camera paired with Leica® licensed digital image processing software. No stains were employed so as to not compromise the highly water-sensitive thin-sections. A total of 512 digital images were taken from the 10 thin-section samples. Photomicrograph images were saved as high-resolution jpegs (each circa 4–8 Mb) and then reprocessed in Adobe Photoshop® to enhance color brightness, tone, and contrast. The strategy was to always start at the lowest magnification and to work towards higher and higher magnifications. The maximum magnification was 500× (50× objective paired with 10× oculars). Micromorphological descriptions follow nomenclature and methods presented in Brewer (1976), FitzPatrick (1993) and Stoops (2003).

Bulk paleosol samples were collected at either 3 cm (FLK, E4) or at 5 cm (PTK A, PTK B) depth intervals for bulk geochemistry. Bulk samples of Chapati Tuff collected at 6 locations in the study area were analyzed as representative paleosol parent materials and then averaged as a "model parent material". The GPS locations of the samples are in Supplementary Table 1 and shown in Uribelarrea et al. (2014, his Fig. 1). Results of geochemical analyses of paleosol and Chapati Tuff samples obtained using ICP-MS and ICP-AES from a commercial laboratory (ALS Minerals, Reno, NV) are provided in Supplementary data Appendix 1. Geochemical data were examined using mass-balance and calculation of tau (τ) values was performed assuming immobile TiO_2, following methods outlined in Brimhall and Dietrich (1987), Brimhall et al. (1988, 1991a,b), and Driese et al. (2000) in which: $\tau_{i,j} = \{[(C_{j,w}) / (C_{j,p})] / [(C_{i,w}) / (C_{i,p})]\} - 1$, which uses the concentrations (C) of elements (j) in the parent material (p), relative to an immobile element (i) to establish the mass changes in the progressively weathered material (w).

Previous geochemical research on lower Bed II Olduvai paleosols (Ashley and Driese, 2000) as well as on surface and Holocene buried soils in Kenya (Driese et al., 2004) has shown that TiO_2 is superior over Zr for mass-balance reconstructions in these volcaniclastic-parented soils and paleosols because it is present in much higher abundance than Zr (and hence easier to quantify). TiO_2 is less susceptible to dissolution in the generally alkaline geochemical conditions that prevail at these sites. Work by McHenry (2009) on element mobility during zeolitic and argillic alteration of volcanic ash in Tuff IF at Olduvai Gorge also suggested that, under the likely range of Eh and pH experienced during weathering, TiO_2 is less mobile than Zr and hence constitutes a better choice for geochemical mass-balance requiring an assumption

Please cite this article as: Driese, S.G., Ashley, G.M., Paleoenvironmental reconstruction of a paleosol catena, the Zinj archeological level, Olduvai Gorge, Tanzania, Quaternary Research (2015), http://dx.doi.org/10.1016/j.yqres.2015.10.007

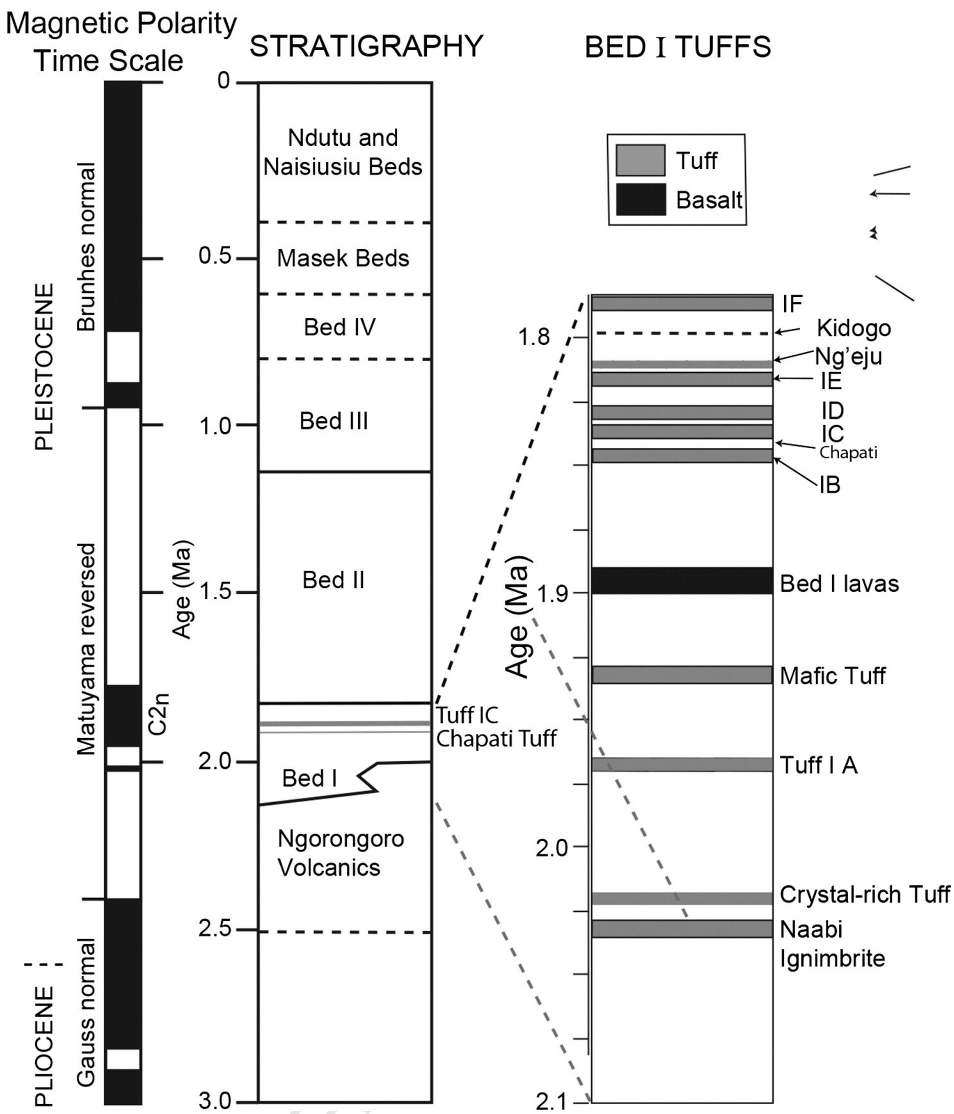

Fig. 3. Stratigraphic column of Bed I at FLK Zinj site and FLK NN showing major tuffs that define chronostratigraphy. Stratigraphic level of Tuff IC and Chapati Tuff are indicated. The age of the Level 22 paleosol catena at the Zinj archeological site, Olduvai Gorge, Tanzania is constrained by Tuff IC dated at 1.84 Ma.

of an immobile element. A standard immobile element cross-plot of wt.% TiO_2 vs. ppm Zr, as well as plots of wt.% TiO_2 and ppm Zr vs. depth, were used to initially compare parent material variability between the four different sites. The parent material was likely from eruptions of Olmoti (McHenry et al., 2008) and from Mg-smectitic clays produced in the lake and deposited on the lake margin (Hover and Ashley, 2003). The Zr/TiO_2–Nb/Y classification diagram from Winchester and Floyd (1977) was also used to classify the parent materials that contributed to paleosol development, in which the various named fields represent the compositional ranges of most volcanic rocks.

Pedotransfer functions (proxies) for paleo-Vertisols

Bulk oxides were used to estimate proxy physical and chemical properties of paleo-Vertisols using regression-based transfer functions presented in Nordt and Driese (2010a). As noted by Nordt et al. (2012, 2013), few "deep time" paleosol researchers routinely submit samples for soil characterization using modern soil methods, and processing lithified paleosols using modern soil characterization methods should only be done with great caution and with the knowledge that some measures will be erroneous because they are modified after soil burial by processes involving diagenesis. The pedotransfer functions of Nordt and Driese (2010a) that are based entirely upon bulk geochemistry were developed for Vertisols and paleo-Vertisols precisely because of these types of problems associated with post-burial processes. Properties estimated included % total clay, coefficient of linear extensibility (COLE), bulk density (BD), cation exchange capacity (CEC), pH, base saturation (BS), dithionite–citrate–extractable iron (Fe_d), exchangeable sodium percentage (ESP), and electrical conductivity (EC). Where formulae utilize more than one oxide, wt.% oxides are all normalized to their respective molecular weights (i.e., converted to moles). Organic carbon (Org. C) and organic nitrogen (Org. N) were estimated using the ppm Pb-based pedotransfer function presented in Nordt et al. (2012). These estimated physical and chemical properties are important in evaluating soil fertility and ecosystem function. For information on how these properties are measured in modern soils see the Soil Survey Laboratory Methods Manual (Soil Survey Staff, 2004).

Mean annual precipitation (MAP)

Mean annual precipitation (MAP) was estimated using the Chemical Index of Alteration minus Potassium (CIA-K) proxy of Sheldon et al. (2002), which is defined as $100 \times [(Al_2O_3) / (Al_2O_3 + Na_2O + CaO)]$, and where the oxides are all normalized to their respective molecular weights (i.e., converted to moles). This CIA-K proxy is mainly a measure of clay formation and base loss associated with feldspar weathering. It

Please cite this article as: Driese, S.G., Ashley, G.M., Paleoenvironmental reconstruction of a paleosol catena, the Zinj archeological level, Olduvai Gorge, Tanzania, Quaternary Research (2015), http://dx.doi.org/10.1016/j.yqres.2015.10.007

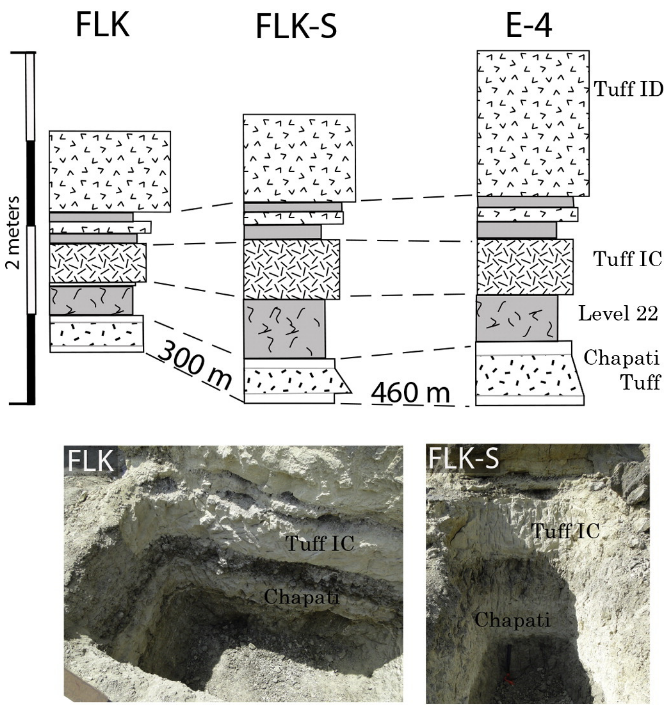

Fig. 4. Stratigraphic context of the paleosol (Level 22) is depicted in the FLK and E4 study areas and in an exposure (FLK-S) in between. The location of the ~0.76-km-long transect is shown on location map (Fig. 2). The paleosol varies in thickness from <20 cm to >30 cm. The Chapati Tuff immediately underlies Level 22 paleosol and Tuff IC caps it. Contacts are nearly always sharp. Photos of trenches show parallel, flat bedding typical of the area. A photograph of E4 is not available.

was designed to be universal for application to well-drained B horizons for all paleosol types in which there has been sufficient time of soil formation to equilibrate with climate conditions. A second paleoprecipitation proxy used in this study is CALMAG of Nordt and Driese (2010b), which is defined as $100 \times [(Al_2O_3) / (Al_2O_3 + CaO + MgO)]$, and where all of the oxides are normalized to their respective molecular weights (i.e., converted to moles) and the paleosol contains less than 10% CaO. This CALMAG proxy is mainly a measure of loss of exchangeable base cations in Vertisols associated with increased rainfall, and was designed for application to well-drained B horizons of paleo-Vertisols. The Chemical Index of Alteration (CIA) proposed earlier by Nesbitt and Young (1982) and Maynard (1992), which is defined as $100 \times [(Al_2O_3) / (Al_2O_3 + CaO + Na_2O + K_2O)]$, was also used to evaluate the degree of weathering of the paleosols.

Two newly proposed chemical weathering indices (Babechuk et al., 2014), (1) the Mafic Index of Alteration (MIA), which is defined as $100 \times [(Al_2O_3 + Fe_2O_{3(T)}) / (Al_2O_3 + Fe_2O_{3(T)} + MgO + CaO^* + Na_2O + K_2O)]$, where $Fe_2O_{3(T)}$ is the total iron measured as Fe_2O_3 and CaO^* is the CaO not residing in carbonate minerals, and (2) the Index of Lateritization (IOL), which is defined as $100 \times [(Al_2O_3 + Fe_2O_{3(T)}) / (SiO_2 + Al_2O_3 + Fe_2O_{3(T)})]$, were used to evaluate the intensity of trachyte basalt parent material weathering. In the case of MIA, molar ratios of the major element oxides are calculated by converting wt.% concentrations into moles. In the case of IOL the mass (wt.%) ratios of SiO_2, Al_2O_3, and $Fe_2O_{3(T)}$ are used in the calculations.

Results

Stratigraphy

Stratigraphic context for Level 22 is shown in Fig. 4 (see location map Fig. 2 for line of transects). In ascending stratigraphic order, Chapati Tuff is a white to light yellow to light gray colored, laminated tuff composed of three layers. The basal contact is sharp and from the bottom is A) a thin (1–4 cm) silty tuff, overlain by B) a thick (10–25 cm) partially reworked, vitric tuff containing rock fragments and glass shards, mainly massive but locally laminated, overlain by C) a thin (2–6 cm) bed with pumices and carbonate blebs (Fig. 4). The Chapati Tuff was first described by Uribelarrea et al. (2014). Its composition is plagioclase, augite, and iron and titanium-rich magnetite similar to many other Bed I tuffs (Hay, 1976; McHenry, 2004).

Level 22 paleosol is a clay deposit ranging from less than 20 cm to slightly greater than 30 cm thick. Most localities display two layers: a lower layer with ~75–90% clay and an upper layer with ~60–70% clay (Fig. 4). Both layers have well-developed paleosol structures, including weak medium prismatic peds, parting to fine to medium, subangular blocky peds, as well as common shiny slickenside planes. The upper unit has more abundant carbonate rhizoliths and nodules, as well as siliceous root traces and fine to medium, subangular blocky peds with some small slickensides. Munsell colors reflect the difference in grain size and pedogenic modification: the bottom is dark olive gray, 5Y 3/2 and the top is olive, 5Y 4/2. Level 22 has been similarly described by Uribelarrea et al. (2014). Level 22 at PTK (B) is distinctly different. The concentration of opaline silica (silicified plant remains, phytoliths and diatoms) is dramatically increased in both layers changing the color to a light gray (5Y 7/2) (Fig. 5).

Tuff IC is an airfall deposit that is relatively constant in thickness (30–35 cm) throughout the study area (Fig. 4). It is medium- to coarse-grained vitric tuff of trachyte composition (Hay, 1976) and is typically root marked. The bottom contact is sharp and at FLK blanketed fossils and bones lying on the surface creating an archeological site with excellent preservation.

Micromorphology

A summary that includes important thin-section observations is presented in Table 1. Examination of thin sections revealed a variety of pedogenic features clearly visible at the microscale of the Zinj Level 22 paleosol (Figs. 6, 7). Features common to all four sites included moderately weathered feldspars and highly weathered volcanic rock and tephra grains, highly weathered ferromagnesian silicate grains, and a >30% clay (smectite) matrix component. At the PTK A site, located about 1.5 m away from siliceous "earthy clay" deposit (Fig. 5), root traces and soil animal burrows with fecal pellets are common in the paleosol, clay matrix content is high, and the clays exhibit sepic–plasmic (bright-clay) microfabrics (Fig. 6A–D). Volcanic rock fragments and feldspars are hydrolyzed and altered to clay minerals and zeolites (Fig. 6C–D). The zeolites fill pore spaces are up to 10–20 μm in diameter, are anhedral to subhedral in shape, and exhibit very low birefringence. The paleosol matrix at PTK B (Fig. 5) is siliceous earthy claystone (rather

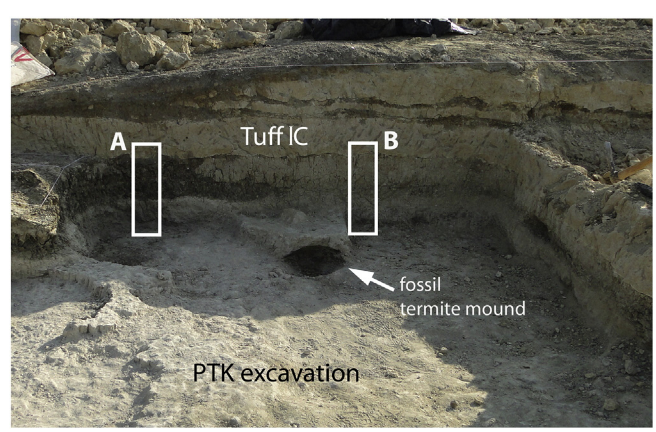

Fig. 5. Field photograph showing two paleosol profiles (A, B) sampled at PTK wetland and archeological site, each overlain directly by Tuff IC. Distance between two profiles is less than 1.5 m.

Please cite this article as: Driese, S.G., Ashley, G.M., Paleoenvironmental reconstruction of a paleosol catena, the Zinj archeological level, Olduvai Gorge, Tanzania, Quaternary Research (2015), http://dx.doi.org/10.1016/j.yqres.2015.10.007

Table 1
Comparison showing the distinguishing characteristics of the paleosols at the four Zinj paleosol sites.

Paleosol	PTK A	PTK B	E4	FLK
Paleosol material and source(s) for Chapati Tuff	Waxy clay (trachyte to phonolite source)	Siliceous earthy clay (trachyte to phonolite source)	Waxy clay (trachyte to phonolite source)	Waxy clay (trachyte to phonolite source)
Vertic (shrink–swell) features (field ± thin-section obs.)	Present: slickensides and b-fabrics	Absent	Present: slickensides	Present: slickensides and b-fabrics
Illuviated clays	Absent	Absent	No data	Present
Zeolites	Present	Absent	No data	Present
Base loss	Na, K, Mg losses; 150% Ca gain in subsoil	Na, K, Mg losses; 150% Ca gain upward to surface	Na, K, Ca losses; 150% Mg gain	Na, K, Ca losses (with subsoil Ca gain); 150% Mg gain
Redoximorphy	Fe, Mn, Cr, V losses at surface but 10–75% gains at depth	Fe, Mn losses; 10–50% Cr and V gains	Fe, V losses; 225% Mn gain; 10% Cr gain near top	Fe loss but 25% gain at depth; 50–200% gains in Mn, Cr and V
Immobile elements	Si, Al, Zr, Nb losses with 10–75% gains in Si, Zr and Nb at depth	Si, Al, Nb losses, with 10–50% gains in Zr and Nb at depth	10–100% gains in Si, Al, Zr and Nb gains, increasing towards surface	Si, Al losses at surface; 25–100% gains in Si, Al, Zr and Nb at depth
Feldspar weathering, P biocycling	150% P gain; Ba, Sr, and Rb erratic losses and gains	175% P gain; Ba, Sr, and Rb losses, with gains in subsoil	25% P loss; 25–100% Ba, Sr and Rb upward gains	Ba, Sr and P losses; up to 100% Rb gains in subsoil
Plant micro-nutrient elements	Cu, Ni, Pb, Zn losses towards surface, but with 5–150% gains at depth	Pb and Zn losses; 75–125% gains in Cu and Ni	50–175% gains in Cu and Ni; 25% gain in Zn; Pb loss	Pb and Zn losses; 25–125% gains in Cu and Ni; losses of Pb and Zn; 10–50% gain in Zn at depth

than waxy clay as at PTK A), and there is extraordinary preservation of root fossils by permineralization (silicification) of plant tissues (Fig. 6E, F). In addition, burrows of fossil termites and other soil animals are present and infilled with fecal pellets. Ferromagnesian silicates, as well as feldspars, show a high degree of weathering and alteration to Fe oxides and oxyhydroxides, and to clays and zeolites (Fig. 6G–H). The paleosol at the FLK site, as was the case for the paleosols at PTK A and E4, is dominated by waxy clay that has well-developed sepic–plasmic (bright-clay) microfabrics, but in addition, has abundant root traces coated by yellowish-colored illuviated clay deposits with high birefringence, as well as pedogenic clay deposited on ped faces (Fig. 7A–D). Redox depletions and enrichments occur in association with roots and other macropores (Fig. 7E). Zeolite alteration of lapilli and zeolitized rhizoliths are also present at FLK (Fig. 7F–H). There is a moderate degree of weathering and alteration of feldspars to clays and zeolites, and weathering of ferromagnesian silicates to Fe oxides and oxyhydroxides (Fig. 7G, H).

Whole-rock geochemistry

Bulk geochemical data for the paleosols, as well as for six Chapati Tuff parent material samples, are provided in Supplementary data Appendix 1, and important distinguishing characteristics of the four paleosol sites are summarized in Table 1. Immobile element geochemistry presented in Fig. 8 shows that over the entire Level 22 paleosol catena, Zr has a 2-fold change in concentration from as low as 250 ppm to as high as 500 ppm. In contrast, with the exception of anomalously high TiO_2 concentrations measured from paleosol tops, TiO_2 content ranges from 0.5 to 1.0 wt.%, which is also about a two-fold difference. Because it has a more uniform concentration with depth (Supplementary data Appendix 1), and because the TiO_2 content is so much higher and hence has less relative error associated with measurement, it was assumed to represent an immobile element suitable for use in subsequent mass-balance calculations. Samples collected from the tops of paleosols had much higher TiO_2 contents, ranging from 1.2 to 2.0 wt.% (Fig. 8), far in excess of the average composition of 0.41 wt.% (n = 25) for phenocryst glass from Tuff IC reported by McHenry (2004, 2005). All but one of the six Chapati Tuff samples had immobile element chemistry overlapping with that of the paleosols (Fig. 8), which indicates that it is appropriate for parent material and thus used in subsequent mass-balance calculations.

The Zr/TiO_2–Nb/Y classification diagram from Winchester and Floyd (1977) was used to classify the parent materials that contributed to paleosol development, and indicates that the parent materials were chiefly trachyte and possibly some phonolite. This interpretation is supported by previous work on the phenocryst chemistry of the Olduvai tuffs by McHenry (2004, 2005) and McHenry et al. (2008), with only two samples plotting in the pantellerite field. The SiO_2–Al_2O_3–Fe_2O_3 (SAF) ternary plot of the bulk compositions of the Zinj archeological site paleosols shows no differences between the four sites analyzed (Appendix 1). However, from the Al_2O_3–($CaO + Na_2O$)–K_2O (A–CN–K) plot it is evident that: (1) the bulk compositions of the paleosols at the PTK A and B sites are 10% more potassic than the paleosols at the other sites, and (2) the paleosol at E4 site is 10–15% more aluminous than the paleosols at the other sites (Supplementary data Appendix 1). The bulk compositions of the "waxy clay" identified for the Zinj paleosol at 3 of the 4 sites (FLK, PTK A, E4) and earthy clay identified at site PTK B are well within the compositional ranges for major, minor and trace elements reported by Deocampo et al. (2002) for bulk samples of the two different lithologies; however, the waxy clay closely resembles Deocampo et al.'s (2002) low-Mg basal waxy claystone, whereas the earthy clay at PTK B is 40% lower in Al_2O_3 and 25% higher in CaO than earthy claystone.

Geochemical mass-balance, assuming a model parent material calculated as an average of six samples of Chapati Tuff from across the paleocatena, and assuming that TiO_2 was immobile during weathering, was used to calculate tau (τ) values for major elements as well as for minor elements and some trace elements. The results (not accounting for any volume changes during weathering) show that the paleosols at PTK A and B are generally geochemically similar as examined with mass-balance, in spite of having different soil materials (waxy clay at site A vs. siliceous earthy clay at B). This is exemplified by translocation depth functions for the alkali and alkaline earth elements (approximating exchangeable base cations), which show 25–99% net losses of Na_2O, K_2O, and MgO, and up to 200% net gains of CaO (Fig. 9A, B). Translocation depth functions for the redox-sensitive elements for PTK A and PTK B are also very similar, with 25–50% net losses of Fe_2O_3, MnO, and V, in the upper 10–15 cm, and 25–75% net gains of these same constituents, plus Cr, from 15 to 33 cm depth (Fig. 9E, F). Both PTK A and PTK B paleosols show overall 25–75% net losses of all immobile elements, including SiO_2, Al_2O_3, Zr and Nb (Fig. 9I, J). In addition, the paleosols at both the PTK A and B sites show 25–175% net gains in P_2O_5 towards surface, erratic patterns gains and losses of Sr, losses of Ba and Rb, as well as somewhat similar depth functions of 25–50% net losses for nutrient micro-element/organic C-affinity trace elements such as Pb and Zn, and 50–125% net gains of Cu and Ni (Supplementary Fig. 1A, B, E, F).

Translocation depth functions for the paleosols at the E4 and FLK sites are similar, and are both very different from the translocation

Please cite this article as: Driese, S.G., Ashley, G.M., Paleoenvironmental reconstruction of a paleosol catena, the Zinj archeological level, Olduvai Gorge, Tanzania, Quaternary Research (2015), http://dx.doi.org/10.1016/j.yqres.2015.10.007

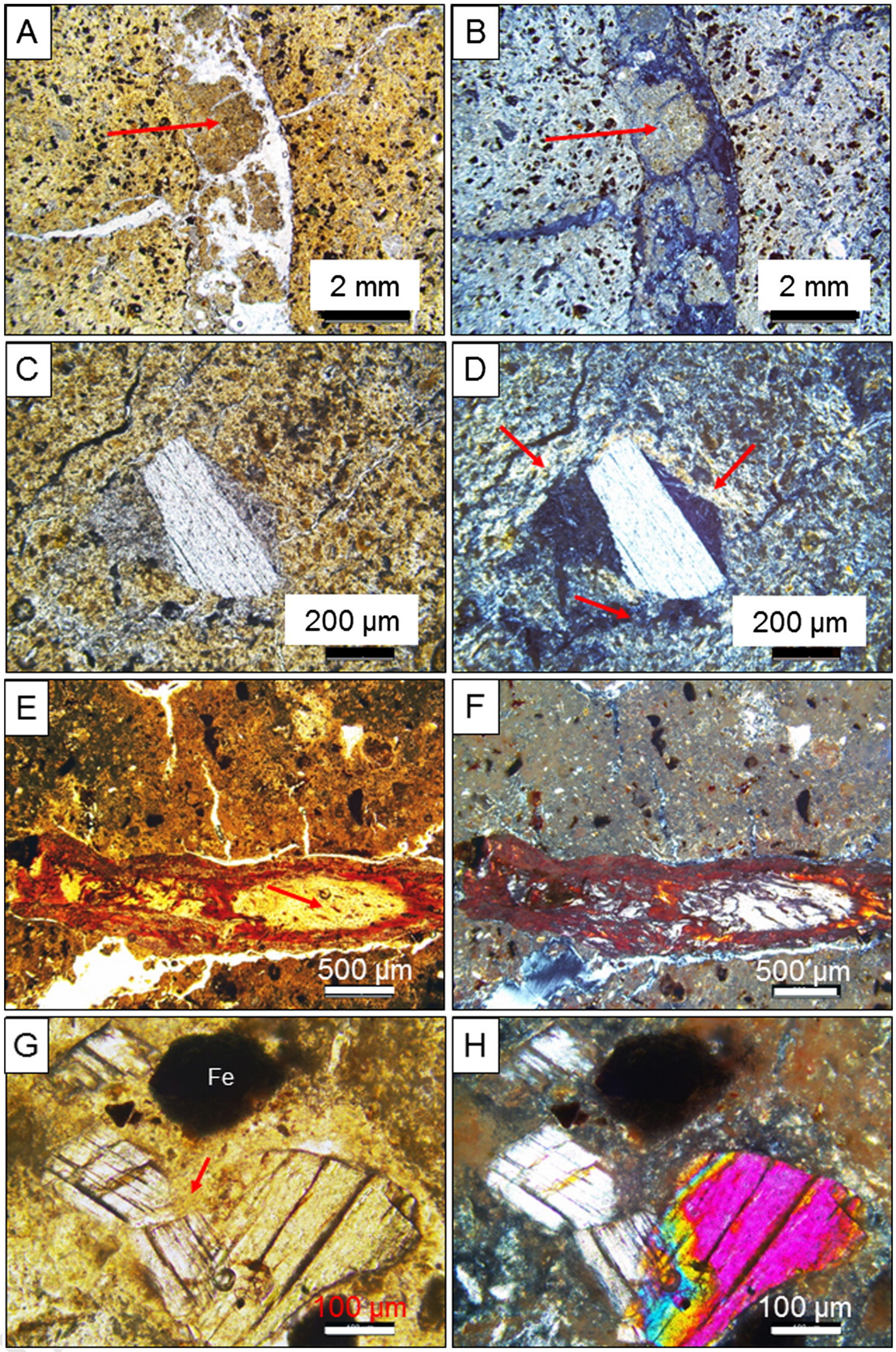

Fig. 6. Examples of micromorphological features in PTK A waxy clay paleosol (A–D) and PTK B earthy clay paleosol (E–H). (A, B) Soil animal burrow partially filled with fecal pellets; note sepic–plasmic (bright clay microfabric visible in (B) resulting from wetting and drying of soil matrix (PPL, XPL)). (C, D) Feldspar phenocryst attached to volcanic rock fragment, in which both show evidence for weathering; note sepic–plasmic (bright clay microfabric visible in (D) produced by wetting and drying cycles (PPL, XPL)). (E, F) Silicified plant root showing unusual preservation of outer xylem (red: yellow arrow) and inner phloem (yellow: red arrow) cells in soil matrix lacking evidence for wetting and drying (PPL, XPL). (G, H) Partially weathered and broken plagioclase feldspar grain (red arrow) alongside partially weathered pyroxene grain (bright interference colors); note opaque dark Fe oxide (Fe) masses that are probably altered ferromagnesian silicates (PPL, XPL). (For interpretation of the references to color in this figure legend, the reader is referred to the web version of this article.)

depth functions for the PTK A and PTK B sites. Depth functions for alkali and alkaline-earth elements at E4 and FLK are similar, showing 150% net MgO accumulation, 10–25% net Na_2O removal and K_2O conservation, and up to 50% CaO accumulation in the subsoil for FLK (Fig. 9C, D). Translocation depth functions for redox-sensitive elements at the E4 and FLK sites are very similar, with 10–20% net loss for E4 (or 10–20% net gain for FLK) of Fe_2O_3, 100–200% net gains of MnO, V and Cr, at the FLK site and conservation to 10–50% net losses of these elements at the E4 site (Fig. 9G, H). Immobile elements show conservation of Al_2O_3, and 25–100% net gains of SiO_2, Zr and Nb (Fig. 9K, L). Translocation depth functions for biocycling and leaching-related elements at the E4 and FLK sites show evidence for 10–25% P_2O_5 removal at surface, up to 100% Rb enrichments, and with variable behavior for Ba and Sr, which are lost (25–50%) at FLK and erratic at E4 (Supplementary

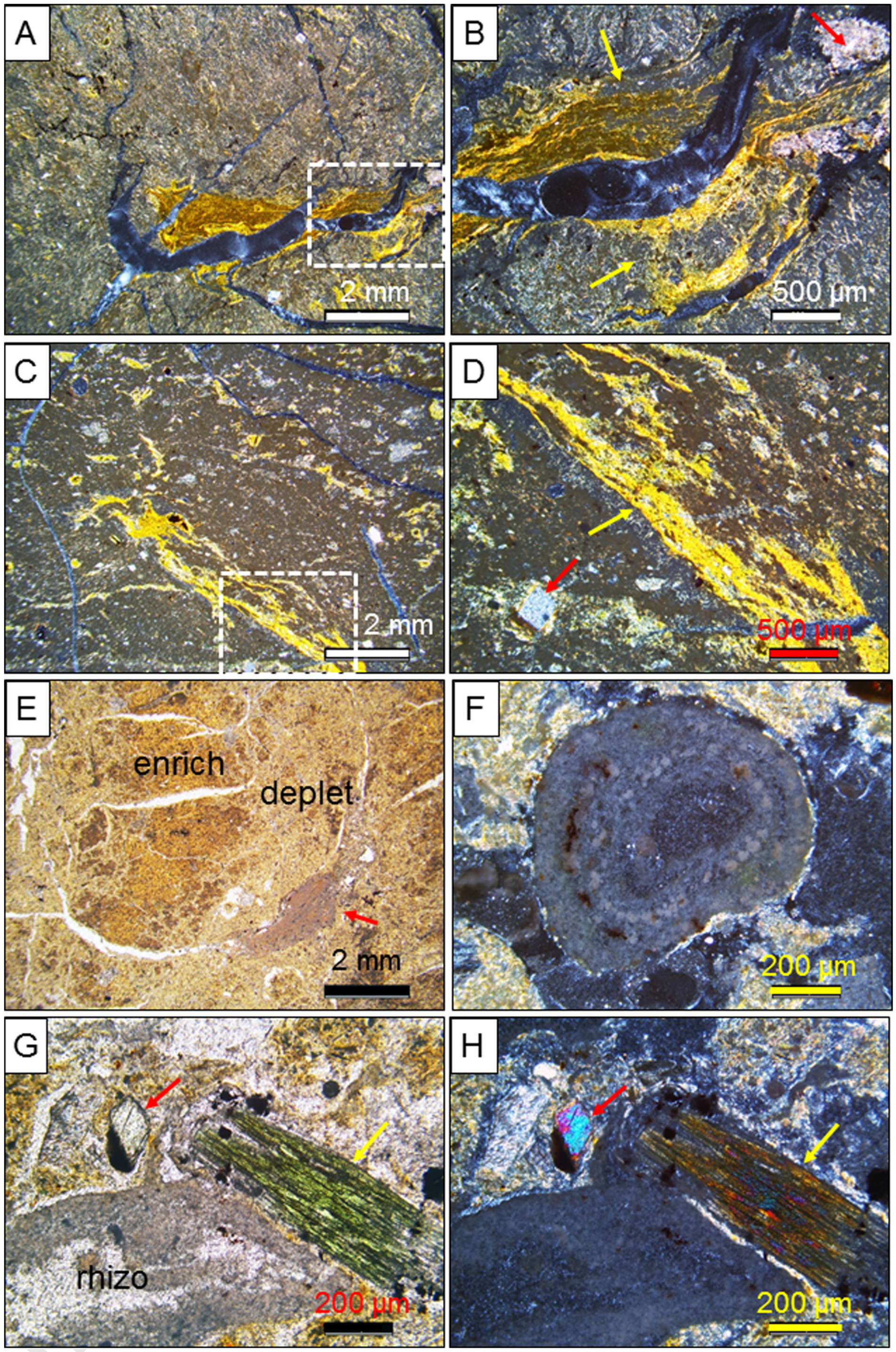

Fig. 7. Examples of micromorphological features in FLK-NN-west wetland and wetland margin paleosol. (A, B) Paleosol with weak sepic–plasmic (bright clay) matrix fabric, but containing high birefringence (yellow) illuviated clay void filling of root pore (yellow arrows), as well as minor amount of calcite microspar (red arrow); both are in XPL, white box inset in (A) shows location of photo (B). (C, D) High birefringence (yellow) illuviated clay void filling of root pore (yellow arrow), as well as minor amount of clay coating quartz grain (red arrow); both are in XPL, white box inset in (C) shows location of photo (D). (E) Redoximorphic features showing redox enrichment (enrich) and redox depletion (deplet) of Fe oxides and oxyhydroxides associated with periodic saturation followed by drying and aeration; note pink-colored zeolite (possibly analcime?) replacing volcanic grain (red arrow) (PPL). (F) Zeolitized lapilli grain showing characteristic low birefringence of zeolites compared to bright birefringence of smectite clays surrounding the grain (XPL). (G, H) Zeolitized rhizolith (gray, low birefringence) and chloritized biotite (yellow arrow), together with partially weathered pyroxene grain (red arrow) (PPL, XPL). (For interpretation of the references to color in this figure legend, the reader is referred to the web version of this article.)

Fig. 1C, D). Both the paleosols at FLK and E4 show similar depth functions for nutrient micro-element/organic C-affinity trace elements with 50–200% net gains of Cu and Ni, and 10–25% net losses of Pb and Zn, with similar gains at depth (Supplementary Fig. 1G, H).

Estimated soil characterization data for paleosols

Soil characterization data estimated for the Zinj archeological site paleosol at FLK, using the Vertisol pedotransfer functions of Nordt and

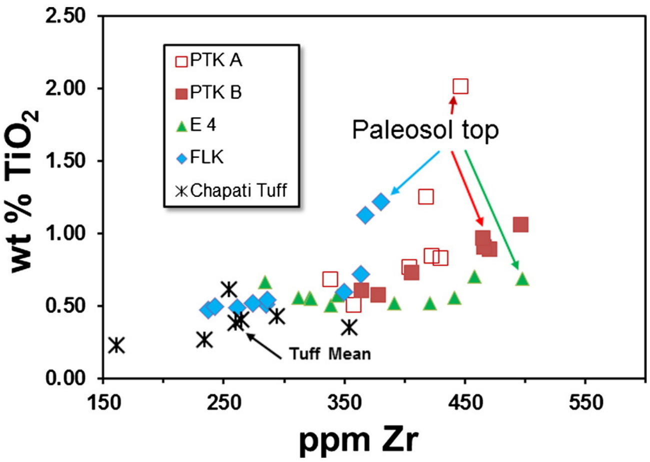

Fig. 8. Immobile element geochemistry of Level 22 Zinj archeological site paleosol at four study sites and six samples of underlying Chapati Tuff used to develop a model parent material (Tuff mean indicated with black arrow). Cross-plot of wt.% TiO_2 vs. ppm Zr shows nearly constant TiO_2 and highly variable Zr contents within each paleosol profile, with the exception of the top portions of each paleosol (denoted by various colored arrows), which show 2–3× TiO_2 enrichment that might be related to inputs from overlying Tuff IC as well as to residual enrichment and concentration of these constituents by weathering.

Driese (2010a), are shown in Tables 2 and 3; the estimated soil characterization data for the Zinj paleosol at sites PTK A and E4 are provided in Supplementary Tables 2 and 3. A comparison of variability of some selected reconstructed characterization properties with depth, as well as between the three paleosol profiles with vertic (Vertisol-like) properties, is shown in Supplementary Fig. 2.

Three of profiles (FLK, E4 and PTK A), in addition to exhibiting Vertisol-like field properties such as slickensides, and micromorphologic features such as sepic-plasmic (bright clay) microfabrics, have the requisite reconstructed high total clay and fine clay contents. They also have the expected high COLE, CEC, BS, and EC indicating very high shrink–swell behavior, for classification as USDA Vertisols, based on current USDA Soil Taxonomy (Wilding and Tessier, 1988; Southard et al., 2011; Soil Survey Staff, 2014). Reconstructed pH for the paleosols, overall, is moderately to strongly alkaline (7.9–8.5) with the estimated pH for the paleosol at the PTK A site being 0.2–0.3 pH units lower than that estimated for the FLK and E4 sites (Supplementary Fig. 2A). The reconstructed $CaCO_3$ content of the paleosols, as would be expected based on field descriptions and thin section study, ranges from 1 to 8 wt.%, with the average estimated $CaCO_3$% for the paleosol at the PTK A site (3.7%) higher than the averages estimated for the paleosols at the FLK and E4 sites (1.4 and 1.0%, respectively) (Supplementary Fig. 2B). The reconstructed organic C % of the Zinj paleosols ranges from 0.24 to 0.69%, and the paleosol at the PTK A site shows the highest average estimated organic C (0.6%) as compared with the paleosols at the FLK and E4 sites (0.41 and 0.5%, respectively)

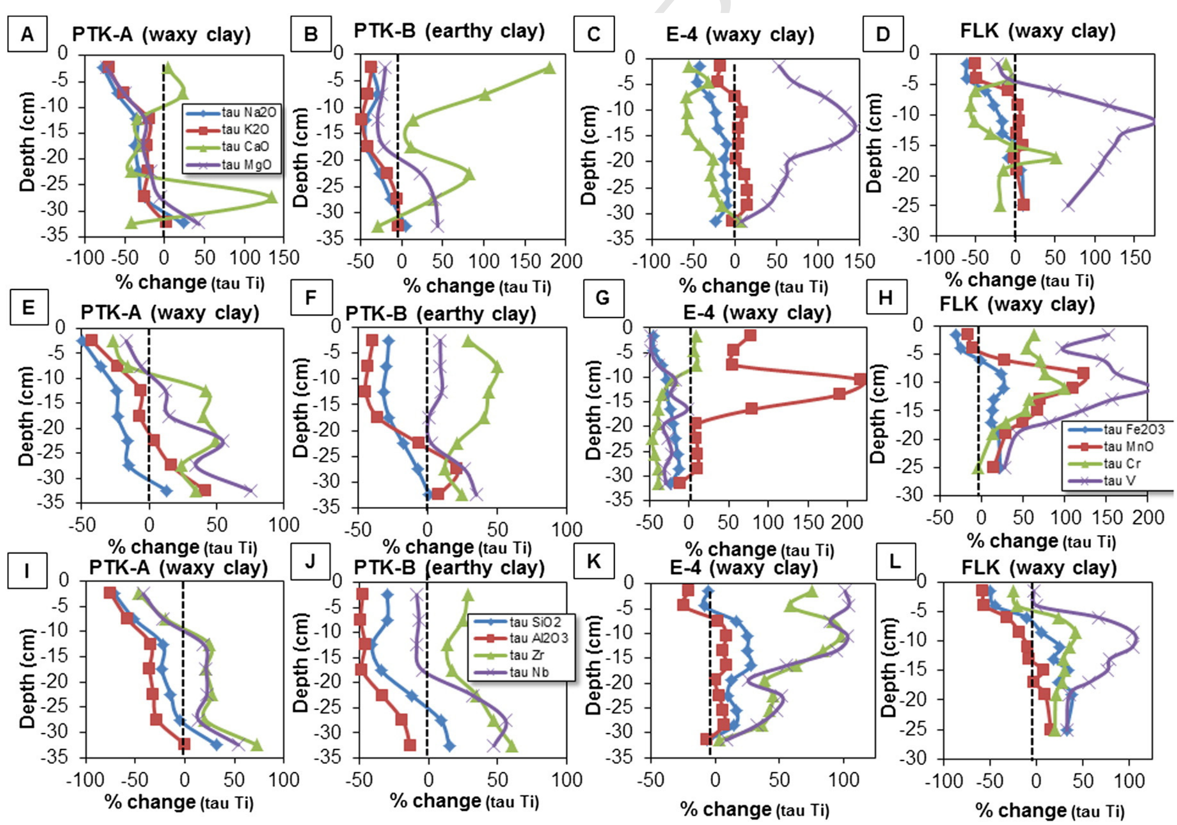

Fig. 9. Mass-balance geochemistry of Level 22 Zinj archeological site paleosols (important trends are summarized in Table 1), normalized to composition of model Chapati Tuff parent material at each site, and assuming immobile TiO_2 during weathering. (A–D) Comparison of translocations for Na_2O, K_2O, CaO and MgO (exchangeable base cations): note that depth patterns for PTK A and PTK B are very similar, with 25–99% net losses of Na_2O, K_2O, and MgO, and large net gains of up to 200% CaO; E4 and FLK, in contrast, both have up to 150% MgO additions, net losses of 25–50% Na_2O, conservation of K_2O, general 25–50% CaO loss for E4 and FLK, but also with a 50% subsoil CaO accumulation for FLK at 17 cm depth. (E–H) Comparison of translocations for Fe_2O_3, MnO, V, and Cr (redox-sensitive major and trace elements): note that depth patterns for PTK A and PTK B are somewhat similar, with PTK A showing 25–50% net losses of Fe_2O_3, MnO, Cr and V at the surface, and net gains of 25–75% of these same constituents at depths of 10–33 cm; in contrast, PTK B has 25–50% losses of Fe_2O_3 and MnO and 10–50% net gains of Cr and V; E4 shows up to 200% net gain of MnO and 25–50% net losses of Fe_2O_3, Cr and V; FLK calculations indicate 100–200% additions of MnO, Cr, and V, and overall conservation to 25% net gain of Fe_2O_3. (I–L) Comparison of translocations for SiO_2, Al_2O_3, Zr and Nb (immobile/resistant major and trace elements): note that depth patterns for PTK A and PTK B are very similar, with 25–75% losses of all immobile elements (except Zr in PTK B) at the surface and 10–60% net gains at depths of 10–33 cm; FLK and E4 show conservation of Al_2O_3 and 25–100% net gains of all immobile/resistant elements at all depths except for losses in the upper 5 cm of each profile.

Please cite this article as: Driese, S.G., Ashley, G.M., Paleoenvironmental reconstruction of a paleosol catena, the Zinj archeological level, Olduvai Gorge, Tanzania, Quaternary Research (2015), http://dx.doi.org/10.1016/j.yqres.2015.10.007

Table 2
Estimated soil characterization data for FLK Zinj site paleosol using Vertisol pedotransfer functions of Nordt and Driese (2010a).

Paleosol horizon (SE)	Clay (%) <5%CaO (±4)	Clay (%) <10%CaO (±5)	COLE ($cm\ cm^{-1}$) <10% CaO (±0.019)	BD ($g\ cm^{-3}$) Noncalc. (±0.1)	CEC ($cmol_c\ kg^{-1}$) <10%CaO (±8)	pH (H_2O) <30%CaO (±0.6)	BS (%) <30%CaO (±8)	$CaCO_3$ (%) <30%CaO (±4%)	Fe_d (%) <30%CaO (±0.4)	ESP (%) <30%CaO (±4)	EC ($dS\ m^{-1}$) <30%CaO (±3)	Org. C (%) (±0.53)	Org. N (%) (±0.04)	Depth (cm)
	46	47	0.12	1.17	43	8.3	111	2.8	2.9	79	181	0.37	0.07	−1.5
	45	46	0.13	1.17	43	8.3	112	2.8	2.8	78	176	0.44	0.08	−4
	44	46	0.13	1.20	43	8.3	111	1.0	1.8	79	180	0.44	0.08	−6
	44	46	0.13	1.19	43	8.4	113	0.7	2.0	78	177	0.53	0.09	−8.5
	43	45	0.13	1.20	43	8.5	114	0.7	1.4	79	181	0.38	0.07	−11
	45	46	0.13	1.20	43	8.4	113	1.0	1.3	80	183	0.34	0.06	−13
	46	47	0.13	1.21	43	8.3	111	1.2	1.0	83	195	0.32	0.06	−15
	45	47	0.13	1.20	43	8.4	112	2.1	1.1	82	194	0.35	0.06	−17
	46	47	0.14	1.22	43	8.2	109	1.1	1.1	86	208	0.40	0.07	−19
	49	50	0.13	1.21	44	8.1	107	1.1	1.2	83	194	0.51	0.09	−25

(Notations: SE = standard error of regression; COLE = coefficient of linear extensibility; BD = bulk density; CEC = cation exchange capacity; BS = base saturation; Fe_d = dithionite–citrate extractable iron; ESP = exchangeable sodium percentage; EC = electrical conductivity; Org. C = organic carbon; Org. N = organic nitrogen).

(Supplementary Fig. 2C). The paleosols all have high reconstructed Fe_d, with Fe_d % the highest for the paleosol at the PTK A site (up to 4%); both the PTK A and FLK paleosols show higher estimated Fe_d in the upper 10–15 cm of the paleosol profiles (Supplementary Fig. 2D). The estimated ESP % of all of the paleosols is very high and ranges from 58 to 108, with somewhat higher average estimated ESP % for the paleosol at the PTK A site (88.7%, vs. 67.9% at E4 and 80.8% at FLK) (Supplementary Fig. 2E). Further estimation of individual exchangeable base cations shows very high exchangeable Ca^{2+} and Mg^{2+}, and relatively high Na^+, and K^+, as well as high sum of exchangeable bases, with the highest estimates reconstructed for the paleosol at the PTK A site, up to 175 $cmole_c$/kg of soil (Supplementary Fig. 2F).

Estimated MAP for paleosols

Mean annual precipitation (MAP) estimated for the Zinj archeological site paleosols at the four sites using the Chemical Index of Alteration minus Potassium (CIA-K) of Sheldon et al. (2002) ranged from 733 to 944 mm/yr, with a standard error of ±172 mm/yr (Table 4). Paleoprecipitation estimated using the CALMAG proxy of Nordt and Driese (2010b) ranged from 742 to 889 mm/yr, with a standard error of ±108 mm/yr (Table 4). Whereas the MAP estimate based on CALMAG was higher than the CIA-K estimate for the PTK A and PTK B paleosol sites, and the MAP estimate based on the CALMAG proxy was lower than that based on CIA-K for the E4 and FLK sites, all differences are within one standard error and thus are not significantly different. All of these estimates for MAP lie within modern udic (or udic–ustic borderline) moisture regimes as classified by the USDA (Soil Survey Staff, 2014).

The Chemical Index of Alteration (CIA) proposed earlier by Nesbitt and Young (1982) and Maynard (1992), and the Mafic Index of Alteration (MIA) and Index of Lateritization (IOL) of Babechuk et al. (2014) all indicated weak to moderate chemical weathering of the Zinj paleosols at the four sites (Table 4). The range of CaO and MgO concentrations for the waxy clay-parented paleosols with vertic (Vertisol-like) properties (PTK A, FLK, and E4) were generally within the CaO range judged acceptable by Nordt and Driese (2010b) for use of the CALMAG proxy (<4%), however all three of the paleosols have MgO concentrations greater than 3.0 wt.% MgO considered the upper limit by Nordt and Driese (2010b; see Supplementary data Appendix A), hence the CALMAG-based proxy estimates for MAP presented in Table 4 should be viewed with caution.

Interpretations and discussion

Micromorphology

Silicified roots, although rare, are certainly *prima facie* evidence for paleosol development (Fig. 6E, F). Similarly, burrows of soil animals infilled with fecal masses, possibly termites, are also strong paleosol indicators (Fig. 6A, B). Based on widespread sepic–plasmic (bright clay or b-fabrics) microfabrics characterized by domains of birefringent clays and the presence of substantial crack-related macropores, the Zinj archeological site paleosols (with the exception of PTK B, a siliceous earthy clay) are unequivocally assignable to the Vertisol soil order (Figs. 4–6) (Brewer, 1976; Wilding and Tessier, 1988; Fitzpatrick, 1993; Stoops, 2003). B-fabric develops in clayey soils as a result of shrink–swell processes related to wet/dry cycles, which causes clay particles to align parallel to each other and appear birefringent under cross-polarized light (Fitzpatrick, 1993). Parallel-striated b-fabric (one direction of preferred clay orientation) is more common; however granostriated b-fabric, (b-fabric developed around grains, peds, or hard Fe–Mn masses where stress due to clay expansion is high) is present in surrounding detrital silicate mineral grains (Figs. 6A–D; 7A–D). Notable is the absence of these types of fabrics in the PTK B paleosol formed from siliceous earthy clay, which lacked the necessary clay

Table 3
Exchangeable base cations estimated for FLK site Zinj paleosol using Vertisol pedotransfer functions of Nordt and Driese (2010a).

Paleosol horizon (SE)	Ex. Ca^{2+} ($cmole_c\ kg^{-1}$) ± 3.9	Ex. Mg^{2+} ($cmole_c\ kg^{-1}$) ± 3.2	Ex. Na^+ ($cmole_c\ kg^{-1}$) ± 1.0	Ex. K^+ ($cmole_c\ kg^{-1}$) ± 0.4	Sum of bases	BS (%) < 30%CaO (±8)	$CaCO_3$ (%) < 30%CaO (±4%)	Depth (cm)
	51.0	52.4	9.4	2.5	115	111	2.8	−1.5
	50.3	56.6	8.9	2.4	118	112	2.8	−4
	20.2	59.1	8.9	2.7	91	111	1.0	−6
	15.9	71.4	8.7	2.6	99	113	0.7	−8.5
	15.2	77.1	8.4	2.3	103	114	0.7	−11
	20.5	69.8	9.0	2.3	102	113	1.0	−13
	24.9	60.1	9.8	2.2	97	111	1.2	−15
	38.6	61.2	9.5	2.2	111	112	2.1	−17
	22.2	53.5	10.1	2.0	88	109	1.1	−19
	21.9	45.3	10.6	2.3	80	107	1.1	−25

Notations: SE = standard error of regression; BS = base saturation.

Please cite this article as: Driese, S.G., Ashley, G.M., Paleoenvironmental reconstruction of a paleosol catena, the Zinj archeological level, Olduvai Gorge, Tanzania, Quaternary Research (2015), http://dx.doi.org/10.1016/j.yqres.2015.10.007

Table 4
Comparison of proxy estimates of MAP and weathering indices for Zinj paleosol sites.

Zinj site	Proxy	Chemical index of alteration minus-potassium (CIA-K)[1]	CALMAG index for Vertisols[2]	Chemical index of alteration (CIA)[3]	Mafic index of alteration (MIA)[4]	Index of lateritization (IOL)[4]
PTK A	Index	57	58	50	52	19
PTK A	MAP	773 mm/yr ± 172 mm	889 mm/yr ± 108 mm			
PTK B	Index	54	54	48	48	18
PTK B	MAP	739 mm/yr ± 172 mm	784 mm/yr ± 108 mm			
E 4	Index	69	57	59	52	19
E4	MAP	944 mm/yr ± 172 mm	869 mm/yr ± 108 mm			
FLK	Index	64	52	55	50	19
FLK	MAP	876 mm/yr ± 172 mm	742 mm/yr ± 108 mm			

Notations: MAP = mean annual precipitation (in mm/yr). References: [1](Sheldon et al., 2002); [2](Nordt and Driese, 2010b); [3](Nesbitt and Young, 1982; Maynard, 1992); [4](Babechuk et al., 2014).

mineralogy and soil moisture deficits to promote high shrink–swell activity (Fig. 6E–H).

Illuviated clay forms when soil waters translocate clay downward through the profile and the clay particles plate out on pore walls as a result of matric forces pulling infiltrating water out of pores and into matrix, or electrostatic forces that exist between the positive and negatively charged surfaces of clays (Fitzpatrick, 1993; Turk et al., 2011). Illuviated clay appears prominently in the FLK profile as gold-colored, highly birefringent accumulations that fill pores and cracks, or coat ped faces (Fig. 7A–D). These pedofeatures in FLK co-occur with zeolitized rhizoliths and lapilli (also occurring in PTK A) that either reflect pedogenic formation under very alkaline soil pH (cf. Ashley and Driese, 2000) or early diagenetic alteration occurring after burial of the paleosol and associated with deposition of Tuff IC (Hay, 1963; cf. McHenry, 2009) (Fig. 7E–H). It is notable that illuviated clays were not observed in thin sections from the PTK A and PTK B profiles, perhaps due to poorer drainage and wetter soil conditions (Fig. 6).

Glaebules and masses of Fe oxide and oxyhydroxide (hematite, plus limonite, goethite or lepidocrocite) occur as clusters of poorly crystalline and opaque, reddish-brown material that appears to pseudomorph (or partially replace) primary ferromagnesian silicate minerals (Figs. 6E–H; 7G, H), all of which would require soil moisture sufficient for mineral weathering. Redoximorphic features, such as Fe–Mn depletions and enrichments of the soil matrix, although less common (Fig. 7E), also require at least seasonal saturation and aeration (Vepraskas, 1996; Vepraskas and Faulkner, 2001). The presence of redoximorphic features (redox depletions and enrichments) indicating seasonal saturation suggests either a udic soil moisture regime in which the soil was generally seasonally moist and never dry for >90 days per year, or a udic–ustic regime in which the soil was generally moist for at least 180 days per year (Soil Survey Staff, 2014). Weathered detrital feldspar grains exhibiting etching, leaching and pitting also attest to soil moisture adequate for substantial hydrolysis (Fig. 6C, D, G, H).

Geochemistry

The immobile element chemistry suggests a uniform trachyte to phonolite parent material for the three waxy clay paleosol profiles (PTK A, E4, and FLK) as well as for the siliceous earthy clay paleosol (PTK B), with some evidence for 2–3× higher TiO_2 and Zr contents at the very tops of the profiles (Table 1; Fig. 8) that might be attributable to residual enrichment during weathering or to additions of these elements associated with emplacement of the overlying Tuff IC. A comparison of the geochemistry of the PTK A and PTK B profiles, which formed laterally adjacent to each other and only separated by 1.5 m, shows: (1) the depth functions for the two profiles for the alkali and alkaline-earth elements are similar and both show losses of three (Na_2O, K_2O, MgO), except for leaching and accumulation of CaO with depth in the PTK A profile and overall upward increases (to 200%) in CaO content for the proximal to spring PTK B paleosols; (2) the depth functions for immobile/resistant and redox-sensitive elements are very similar for both profiles, suggesting maintenance of higher soil moisture and seasonal saturation; (3) both profiles show 150–200% gains in P_2O_5 towards the surface, which could also be associated with surface organic accumulation; and (4) both profiles show similar depth functions for nutrient micro-element/organic C affinity trace elements (Fig. 9A, B, E, F, I, J; Supplementary Figs. 1A, B, E, F).

For the E4 and FLK profiles there are also depth functions common to both profiles: (1) the depth functions for the two profiles for the alkali and alkaline-earth elements are similar, with both showing MgO accumulation, Na_2O and K_2O removal, and greater accumulations of CaO the subsoil for FLK; (2) the depth functions for immobile/resistant and redox-sensitive elements are very similar, suggesting good drainage and soil aeration; (3) both profiles show evidence for biocycling of P_2O_5 (removal at the surface by plants); and (4) both show similar depth functions for nutrient micro-element/organic C-affinity trace elements (Fig. 9C, D, G, H, K, L).

The differences between the two geochemically defined pairs of soil profiles are significant from a paleolandscape and paleohydrologic perspective. The FLK paleosol site has been previously interpreted as recording a paleo-woodland fed with a freshwater spring and wetland 200 m to the north (Ashley et al., 2010a,b,c, 2014b). The E4 and FLK paleosol profiles are much better-developed (i.e., more mature), with a higher degree of geochemical differentiation reflecting more thorough leaching and concentration of mobile constituents with depth, than the PTK A and PTK B profiles (Table 1). The PTK A and PTK B profiles show more overall concentration of CaO compared to losses or leaching of CaO in the E4 and FLK profiles. There is more evidence for immobile element accumulation in the E4 and FLK profiles, whereas immobile element losses characterize the PTK A and PTK B profiles, perhaps reflecting maintenance of chemical conditions more conducive to their mobility (see McHenry, 2009). Proximity to spring seeps and sources of supplemental soil moisture can help explain some of these differences because additions of spring-delivered constituents, such as CaO, can affect transport functions for other elements by a “dilution effect” that diminishes concentrations of other constituents.

Estimates of soil characterization data

Vertisols are a soil order typified by high clay content, with >30% clay and a significant fine clay fraction, and with the clay mineralogy dominated by clays with a high shrink–swell potential (Ahmad, 1983, 1996; Wilding and Tessier, 1988; Southard et al., 2011; Soil Survey Staff, 2014). Pedotransfer function results indicate 45–49% total clay percentages, and high coefficient of linear extensibility (COLE) values, all of which suggest the paleosols were originally dominated by high shrink–swell clays such as smectites (Table 2; Supplementary Tables 2, 3). Vertic features (slickensides) previously identified in the field in all three waxy clay profiles (PTK A, E4, and FLK), as well as in thin sections (b-fabrics) from PTK A and FLK, also point to a clay mineralogy dominated by smectite. Smectite has a high cation exchange capacity (CEC: up to 200 cmolc/kg) compared to other clay types (Brady and Weil, 2002). A dominantly smectite clay mineralogy, combined with high base saturation (BS), and slightly alkaline to alkaline pH estimates indicates that these paleosols had a moderate CEC (average of 43.5 cmolc/kg) and would have readily supported plant growth (Table 2; Supplementary Fig. 2A). Reconstructed organic C percentages average 0.5 wt.% and also suggest maintenance of soil organic matter by growth of vegetation. However, the reconstructed electrical conductivity (EC: averages from 137 to 223), sums of exchangeable bases (Σ bases: averages from 76 to 100), and exchangeable sodium percentage (ESP: averages from 68 to 89%) values are extremely high throughout all three paleo-Vertisol profiles, indicating that soil salinization was a major problem, which could have limited growth of some types of vegetation less tolerant of salinized soils (Tables 2, 3; Supplementary Fig. 2E, F) (Brady and Weil, 2002). Reconstructed soil pH values for the paleosols normally increase in the horizons with greater pedogenic calcite % because of the acid-neutralizing capabilities of calcite; however in this study the PTK A profile, which has higher reconstructed $CaCO_3$%, has a lower reconstructed pH because of the preponderance of MgO held in the smectite mineralogy. Reconstructed Fe_d (Fe extractable from Fe oxides and oxyhydroxides) values are relatively high for all three paleo-Vertisols (Supplementary Fig. 2D), reflecting the formation of Fe glaebules and masses from weathering of primary ferromagnesian silicate minerals described previously in the thin sections.

Paleoenvironment and ecosystem reconstructions

The interpreted paleoenvironmental reconstruction for the paleosol catena at the Zinj Level 22 archeological site at Olduvai Gorge, Tanzania is summarized in Fig. 10, which shows low-precipitation and high-precipitation states for paleo-Lake Olduvai and important influences of fault-controlled spring systems. Based on Magill et al. (2013b) the playa lake flooded the lake margin frequently; more frequently and for longer periods during wet parts of Milankovitch cycles (700 mm/yr) and less frequently and for shorter time periods during dry portions (250 mm/yr) of the Milankovitch cycle. Higher paleosol proxy estimates for MAP of 700–900 mm/yr (Table 4, this study) during low lake level could reflect supplementation of soil moisture by spring discharge and seeps, as suggested in a general model for African Pleistocene–Holocene wetland soils by Ashley et al. (2013). Beverly et al. (2014) reconstructed paleoprecipitation, using the CIA-K bulk geochemical proxy, ranging from 500 to 725 mm/yr (and mainly between 500 and 600 mm/yr), for a suite of paleo-Vertisols formed in the slightly younger, circa 20,000 yr duration interval between the Ng'eju Tuff and Tuff IF (dated at 1.785 Ma) during a precession-influenced hydrological cycle of initially lower, then higher, followed by lower lake levels (Ashley et al., 2014a). Beverly et al. (2014) reported spring tufa deposits at the FLK-1 and OLD-1 sites, but neither at OLD-3 nor at OLD-2, showing that bias towards interpreting higher paleo-MAP from paleosols can be introduced when localized water sources are present.

The relationship between the paleosols, archeological sites, and fault-controlled spring systems is especially apparent in the plan-view map of the sites (Fig. 2). The four paleosol sites (PTK A, PTK B, FLK and E4) define a paleocatena, or ancient soil surface and lateral array of soil environments, separated by no more than 1 km laterally. It is possible that each of the four paleosol sites discussed in this paper had a relationship to a nearby fault-controlled spring system, as was inferred by the presence of freshwater spring carbonate "tufa" deposits associated with the FLK site (Ashley et al., 2014c). Of the three types of depositional models for freshwater spring carbonates presented by Ashley et al. (2014b,c), the "Upper Bed I" model that they presented (their Fig. 11B

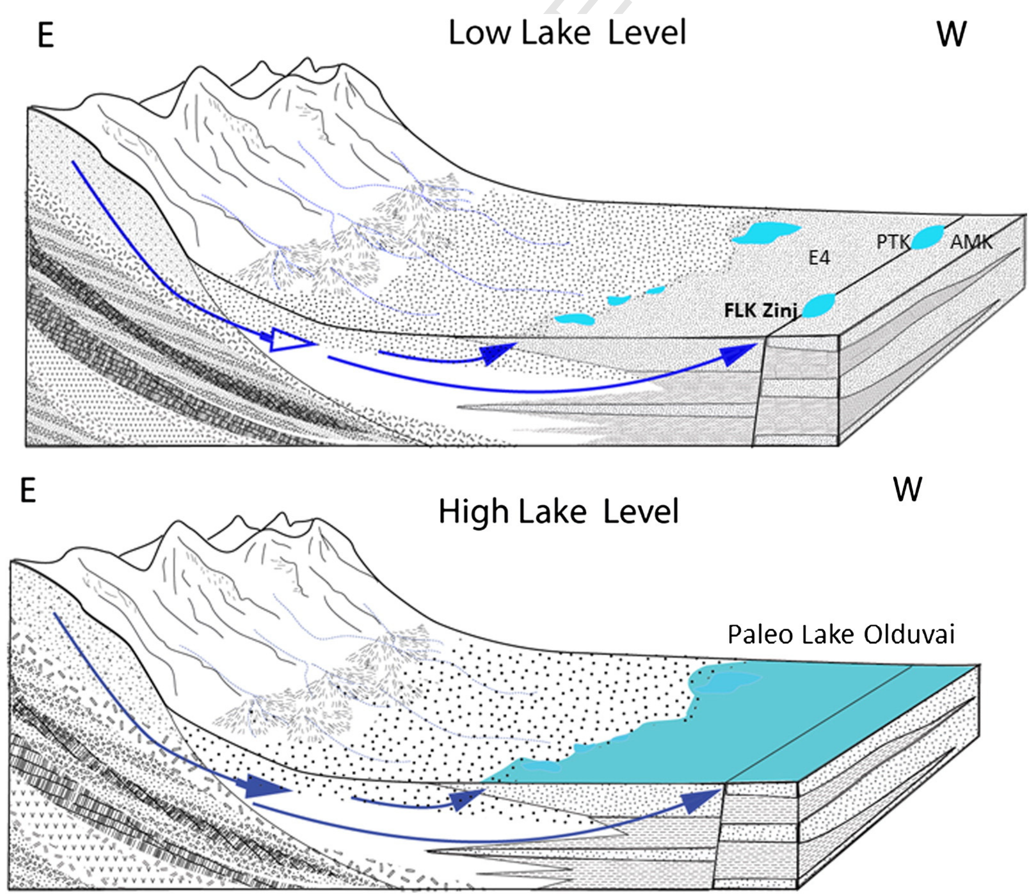

Fig. 10. Reconstruction of paleo-lake Olduvai and influences of fault-controlled spring systems. The playa lake flooded the lake margin frequently; more frequently and for longer periods during wet parts of Milankovitch cycles (700 mm/yr) and less frequently and for shorter time periods during dry portions (250 mm/yr) of the Milankovitch cycle (rainfall estimated by Magill et al., 2013b). Higher paleosol proxy estimates for MAP of 700–900 mm/yr (Table 4, this study) during low lake level reflect supplementation of soil moisture by spring discharge and seeps, which was especially pronounced for paleosols at the PTK A and PTK B sites.

in Ashley et al., 2014c) is most applicable to interpreting the sources for additions of spring seepage along the Zinj Fault to the soils forming at the FLK and PTK sites (Fig. 10), with the soils at the E4 site situated more distal from the Zinj Fault, but possibly proximal to a second fault depicted in Fig. 2 (see also Ashley et al., 2014b, their Fig. 10). Soils arranged across such an envisioned landscape would be expected to show a gradient of soil properties related to declining soil moisture associated with increasing distance from the active spring seeps, as interpreted by Ashley et al. (2014b, their Fig. 10). Some of the variability in micromorphology and geochemistry between the paleosols presented previously could reflect these differences on the paleocatena. For example, the lower pH, higher $CaCO_3$%, higher organic C%, higher Fe_d%, higher ESP, and higher sum of exchangeable bases for the paleosol formed at the PTK A site, as compared with the FLK and E4 site paleosols, could reflect closer proximity to active spring seepage water (Supplementary Fig. 2). To fully explore these ideas further would require excavations targeting the paleosol interval across the landscape in directions perpendicular to the fault traces and away from sections containing evidence for spring tufa deposition.

Summary and conclusions

The results presented here are significant because they show that soil moisture at the four studied sites was supplemented by seepage additions from adjacent springs, and that soil development was enhanced by this additional moisture. Four paleosol profiles within the same stratigraphic horizon that contains the Level 22 Zinj archeological site were examined in middle Bed I at Olduvai Gorge, Tanzania, using a combination of field stratigraphic description, thin-section micromorphology, and whole-rock geochemistry. The analysis provides a rare high-resolution glimpse into the type of landscape hominins we're using. The lateral array of paleosols are interpreted as primarily paleo-Vertisols and represent a soil paleocatena developed on a relatively low-relief, 1.845 Ma paleolandscape for which the precipitation amounts and consequent paleo Lake Olduvai hydrology were affected by precession cycles. During times of higher precipitation (MAP of 700 mm/yr: Magill et al., 2013b) there were lake-level highstands, and waxy clay sediment was deposited in an enlarged saline-lake. During times of reduced precipitation characterized by lake-level lowstands, paleosols formed from these subaerially exposed sediments. Freshwater from fault-controlled springs elevated ambient soil moisture resulting in enhanced pedogenic processes and paleosol development during these lake lowstands, which were much drier periods (MAP of 250 mm/y; Magill et al., 2013b) (Ashley, 2007). This is especially apparent at site PTK where the striking difference in the two paleosols (A) and (B) located <1.5 m apart can be directly attributed to differences in soil moisture levels. Paleosol B developed in a siliceous earthy clay with copious evidence of plants (macro and micro), which reflects the greater proximity of paleosol B to a freshwater spring. These spring seeps developed across the Olduvai paleolandscape provided a supplemental source of soil moisture that was significant because this localized source potentially enhanced vegetative growth, mineral weathering and soil development. The water source perturbed bulk geochemical proxies for MAP (ranging from 733 to 944 mm/yr) well beyond the expected 250 mm/yr, in addition to providing recurrent sources of potable water for vertebrates as well as early hominins. As noted most recently by Ashley et al. (2010a,b, 2014a,b,c) because paleosols are typically the sediments in which important archeological sites are found, understanding the paleoenvironments recorded by paleosols is crucial to developing search models for discovering new sites. Search models might involve repeated closely-spaced trenching seeking signs of increasing intensity of paleosol development, combined with detailed mapping of faults and freshwater tufa deposits indicating the former presence of spring seeps.

Supplementary data to this article can be found online at http://dx.doi.org/10.1016/j.yqres.2015.10.007.

Uncited references

Blumenschine et al., 1994
Bunn, 2007
Domínguez-Rodrigo and Pickering, 2003
Hay and Kyser, 2001
Isaac, 1978
Potts, 1982
Potts, 1984

Acknowledgments

The raw data presented here were collected under permits from the Tanzania Commission for Science and Technology and the Tanzanian Antiquities Department to TOPPP (The Olduvai Paleoanthropological and Paleoecology Project), PIs M. Domínguez-Rodrigo, A.Z.P. Mabulla and E. Baquedano. We appreciate funding provided by the Spanish Ministry of Education and Science through the European project I + D HUM2007-63815. This study was also supported by NSF-SGP grant (#1349651 to D.M. Deocampo, G.M. Ashley, and J.S. Delaney). We are indebted to the late R.L. Hay for his immense knowledge of the geology of Olduvai Gorge and his generosity in sharing his wisdom. We acknowledge the helpful comments offered by two anonymous reviewers, as well as those of associate editor Vance Holliday.

References

Ahmad, N., 1983. Vertisols. In: Wilding, L.P., Smeck, N.E., Hall, G.F. (Eds.), Pedogenesis and Soil Taxonomy II, the Soil Orders. Elsevier Science B.V., Amsterdam, the Netherlands, pp. 91–124.

Ahmad, N., 1996. Occurrence and distribution of Vertisols. In: Ahmad, N., Mermut, A. (Eds.), Vertisols and Technologies for Their Management: In Developments in Soil Science 24. Elsevier Science B.V., Amsterdam, the Netherlands, pp. 1–41.

Ashley, G.M., 2007. Orbital rhythms, monsoons, and playa lake response, Olduvai Basin, equatorial East Africa (ca. 1.85–1.74 Ma). Geology 35, 1091–1094.

Ashley, G.R., Driese, S.G., 2000. Paleopedology and paleohydrology of a volcaniclastic paleosol: Implications for Early Pleistocene paleoclimate record, Olduvai Gorge, Tanzania. Journal of Sedimentary Research 70, 1065–1080.

Ashley, G.M., Barboni, D., Dominguez-Rodrigo, M., Bunn, H.T., Mabulla, A.Z.P., Diez-Martin, F., Barba, R., Baquedano, E., 2010a. A spring and wooded habitat at FLK Zinj and their relevance to the origins of human behavior. Quaternary Research 74, 304–314.

Ashley, G.M., Barboni, D., Dominguez-Rodrigo, M., Bunn, H.T., Mabulla, A.Z.P., Diez-Martin, F., Barba, R., Baquedano, E., 2010b. Paleoenvironmental and paleoecological reconstruction of a freshwater oasis in savannah grassland at FLK North, Olduvai Gorge, Tanzania. Quaternary Research 74, 333–343.

Ashley, G.M., Domínguez-Rodrigo, M., Bunn, H.T., Mabulla, A.Z.P., Baquedano, E., 2010c. Sedimentary geology and human origins: a fresh look at Olduvai Gorge, Tanzania. Sedimentary Research 80, 703–709.

Ashley, G.R., Deocampo, D.M., Kahmann-Robinson, J.A., Driese, S.G., 2013. Groundwater-fed wetland sediments and paleosols: it's all about water table: in Driese, S.G., Nordt, L.C. (Eds.) New frontiers in paleopedology and terrestrial paleoclimatology. SEPM Special Publication 104, 47–61.

Ashley, G.M., Beverly, E.J., Sikes, N.E., Driese, S.G., 2014a. Paleosol diversity in the Olduvai Basin, Tanzania: effects of geomorphology, parent material, depositional environment, and groundwater. Quaternary International 322–323, 66–77.

Ashley, G.M., Bunn, H.T., Delaney, J.S., Barboni, D., Dominguez-Rodrigo, M., Mabulla, A.Z.P., Diez-Martin, F., Gurtov, A.N., Baluyot, R., Beverly, E.J., Baquedano, E., 2014b. Paleoclimatic and paleoenvironmental framework of FLK North archaeological site, Olduvai Gorge, Tanzania. Quaternary International 322–323, 54–65.

Ashley, G.R., De Wet, C.B., Dominguez-Rodrigo, M., Karis, A.M., O'Reilly, T.M., Baluyot, R., 2014c. Freshwater limestone in an arid rift basin: a Goldilocks effect. Journal of Sedimentary Research 84, 988–1004.

Babechuk, M.G., Widdowson, M., Kamber, B.S., 2014. Quantifying chemical weathering intensity and trace element release from two contrasting basalt profiles, Deccan Traps, India. Chemical Geology 363, 56–75.

Beverly, E.J., Ashley, G.M., Driese, S.G., 2014. Reconstruction of a Pleistocene paleocatena using micromorphology and geochemistry of lake margin paleo-Vertisols, Olduvai Gorge, Tanzania. Quaternary International 322–323, 78–94.

Blumenschine, R.J., Cavallo, J., Capaldo, S., 1994. Competition for carcasses and early hominid behavioral ecology: a case study and conceptual framework. Journal of Human Evolution 27, 197–213.

Brady, N.C., Weil, R.R., 2002. The Nature and Properties of Soils, [Thirteenth Edition]. Pearson Education, Inc., New Jersey (960 pp.).

Brewer, R., 1976. Fabric and Mineral Analysis of Soils, [Second Edition]. R.E. Krieger Publishing Company, New York (482 pp.).

Brimhall, G.H., Dietrich, W.E., 1987. Constitutive mass balance relations between chemical composition, volume, density, porosity, and strain in metasomatic hydrochemical systems: results on weathering and pedogenesis. Geochimica et Cosmochimica Acta 51, 567–587.

Brimhall, G.H., Lewis, C.J., Ague, J.J., Dietrich, W.E., Hampel, J., Teague, T., Rix, P., 1988. Metal enrichment in bauxites by deposition of chemically mature aeolian dust. Nature 333, 819–824.

Brimhall, G.H., Lewis, C.J., Ford, C., Bratt, J., Taylor, G., Warin, O., 1991a. Quantitative geochemical approach to pedogenesis: importance of parent material reduction, volumetric expansion, and eolian influx in laterization. Geoderma 51, 51–91.

Brimhall, G.H., Chadwick, O.A., Lewis, C.J., Compston, W., Williams, I.S., Danti, K.J., Dietrich, W.E., Power, M., Hendricks, D., Bratt, J., 1991b. Deformational mass transfer and invasive processes in soil evolution. Science 255, 695–702.

Bunn, H.T., 2007. Meat made us human. In: Ungar, P. (Ed.), Evolution of the Human Diet. Oxford University Press, Oxford, pp. 191–211.

Bunn, H.T., Kroll, E.M., 1986. Systematic butchery by Plio–Pleistocene hominids at Olduvai Gorge, Tanzania. Current Anthropology 27, 431–452.

Cuthbert, M.O., Ashley, G.M., 2014. A spring forward for hominin evolution in East Africa. PloS One 9, e107358.

Deino, A.L., 2012. $^{40}Ar/^{39}Ar$ dating of Bed I. Olduvai Gorge, Tanzania, and the chronology of early Pleistocene climate change. Journal of Human Evolution 63, 251–273.

Deocampo, D.M., Blumenschine, R.J., Ashley, G.M., 2002. Wetland diagenesis and traces of early hominids, Olduvai Gorge, Tanzania. Quaternary Research 57, 271–281.

Deocampo, D.M., Cuadros, J., Wing-Dudek, T., Olives, J., Amouric, M., 2009. Saline lake diagenesis as revealed by coupled mineralogy and geochemistry of multiple ultrafineclay phases: Pliocene Olduvai Gorge, Tanzania. American Journal of Science 309, 834–868.

Domínguez-Rodrigo, M., Pickering, T.R., 2003. Early hominid hunting and scavenging: a zooarcheological review. Evolutionary Anthropology 12, 275–282.

Domínguez-Rodrigo, M., Barba, R., Egelund, C.P., 2007. Deconstructing Olduvai; A Taphonomic Study of the Bed I Sites Vertebrate Paleobiology and Paleoanthropology Series. Springer, AA Dordrecht, The Netherlands, p. 337+xvi.

Domínguez-Rodrigo, M., Bunn, H.T., Mabulla, A.Z.P., Ashley, G.M., Diez-Martin, F., Barboni, D., Prendergast, M.E., Yravedra, J., Barba, R., Sánchez, P., Baquedano, E., Pickering, T.R., 2010a. New excavations at the FLK *Zinjanthropus* site and its surrounding landscape and their behavioral implications. Quaternary Research 74, 315–332.

Domínguez-Rodrigo, M., Mabulla, A.Z.P., Bunn, H.T., Diez-Martin, F., Baquedano, E., Barboni, D., Barba, R., Domínguez-Solera, S., Sánchez, P., Ashley, G.M., Yravedra, J., 2010b. Disentangling hominin and carnivore activities near a spring at FLK North (Olduvai Gorge, Tanzania). Quaternary Research 74, 363–375.

Domínguez-Rodrigo, M., Pickering, T.R., Almécija, S., Heaton, J.L., Baquedano, E., Mabulla, A., Uribelarrea, D., 2015. Earliest modern human-like hand bone from a new > 1.84-million-year-old site at Olduvai in Tanzania. Nature Communications 6, 7987.

Driese, S.G., Nordt, L.C., 2013. New frontiers in paleopedology and terrestrial paleoclimatology: paleosols and soil surface analog systems: in Driese, S.G., Nordt, L.C. (Eds.), new frontiers in paleopedology and terrestrial paleoclimatology. SEPM Special Publication 104, 1–3.

Driese, S.G., Mora, C.I., Stiles, C.A., Joeckel, R.M., Nordt, L.C., 2000. Mass-balance reconstruction of a modern Vertisol: implications for interpretations of geochemistry and burial alteration of paleoVertisols. Geoderma 95, 179–204.

Driese, S.G., Ashley, G.M., Li, Z.-H., Hover, V.C., Owen, B., 2004. Possible Late Holocene equatorial palaeoclimate record based upon soils spanning the Medieval Warm Period and Little Ice Age, Loboi Plain, Kenya. Palaeogeography, Palaeoclimatology, Palaeoecology 213, 231–250.

Fitzpatrick, E.A., 1993. Soil Microscopy and Micromorphology: New York. John Wiley & Sons (304 pp.).

Hay, R.L., 1963. Zeolitic weathering in Olduvai Gorge, Tanganyika. Geological Society of America Bulletin 74, 1281–1286.

Hay, R.L., 1976. Geology of the Olduvai Gorge. University of California Press, Berkeley (203 pp.).

Hay, R.L., Kyser, T.K., 2001. Chemical sedimentology and paleoenvironmental history of Lake Olduvai, a Pliocene lake in northern Tanzania. GSA Bulletin 113, 1505–1521.

Hover, V.C., Ashley, G.M., 2003. Geochemical signatures of paleodepositional diagenetic environments: a STEM/AEM study of authigenic clay minerals from an arid rift basin, Olduvai Gorge, Tanzania. Clays and Clay Minerals 51 (3), 231–251.

Isaac, G.L., 1978. The food-sharing behavior of protohuman hominids. Scientific American 238.

Kraus, M.J., 1999. Paleosols in clastic sedimentary rocks: their geologic applications. Earth-Science Reviews 47, 41–70.

Leakey, L.S.B., 1959. A new fossil skull from Olduvai. Nature 184, 491–493.

Leakey, M.D., 1971. Olduvai Gorge: Excavations in Beds I and II; 1960–1963. Cambridge University Press, Cambridge, UK (306 pp.).

Liutkus, C.M., Ashley, G.M., 2003. Facies model of a semiarid freshwater wetland, Olduvai Gorge, Tanzania. Journal of Sedimentary Research 73, 691–705.

Liutkus, C.M., Wright, J.D., Ashley, G.M., Sikes, N.E., 2005. Paleoenvironmental interpretation of lake-margin deposits using $\delta^{13}C$ and $\delta^{18}O$ results from Early Pleistocene carbonate rhizoliths, Olduvai Gorge, Tanzania. Geology 33, 377–380.

Magill, C.R., Ashley, G.M., Freeman, K.H., 2013a. Ecosystem variability and early human habitats in eastern Africa. Proceedings of the National Academy of Sciences 110, 1175–1180.

Magill, C.R., Ashley, G.M., Freeman, K.H., 2013b. Water, plants, and early human habitats in eastern Africa. Proceedings of the National Academy of Sciences 110, 1167–1174.

Maynard, J.B., 1992. Chemistry of modern soils as a guide to interpreting Precambrian paleosols. Journal of Geology 100, 279–289.

McHenry, L.J., 2004. Characterization and Correlation of Altered Plio–Pleistocene Tephra Using a "Multiple Technique" Approach: Case Study at Olduvai Gorge, Tanzania. New Brunswick, NJ, Rutgers University, unpublished Ph.D. Dissertation, 382 p.

McHenry, L.J., 2005. Phenocryst composition as a tool for correlating fresh and altered tephra, Bed I, Olduvai Gorge, Tanzania. Stratigraphy 2 (2), 101–115.

McHenry, L.J., 2009. Element mobility during zeolitic and argillic alteration of volcanic ash in a closed-basin lacustrine environment: case study Olduvai Gorge, Tanzania. Chemical Geology 265, 540–552.

McHenry, L.J., Mollel, G.F., Swisher, C.C., 2008. Compositional and textural correlations between Olduvai Gorge Bed I tephra and volcanic sources in the Ngorongoro Volcanic Highlands, Tanzania. Quaternary International 178, 306–319.

Nesbitt, H.W., Young, G.M., 1982. Early Proterozoic climates and plate motions inferred from major element chemistry of lutites. Nature 299, 715–717.

Nordt, L.C., Driese, S.G., 2010a. A modern soil characterization approach to reconstructing physical and chemical properties of paleo-Vertisols. American Journal of Science 310, 37–64.

Nordt, L.C., Driese, S.G., 2010b. New weathering index improves paleorainfall estimates from Vertisols. Geology 38, 407–410.

Nordt, L.C., Driese, S.G., 2013. Application of the Critical Zone concept to the deep-time sedimentary record. Sedimentary Record 11 (3), 4–9. http://dx.doi.org/10.2110/sedred.2013.3.

Nordt, L.C., Hallmark, C.T., Driese, S.G., Dworkin, S.I., Atchley, S.C., 2012. Biogeochemistry of an ancient Critical Zone. Geochimica et Cosmochimica Acta 87, 267–282.

Nordt, L.C., Hallmark, C.T., Driese, S.G., Dworkin, S.I., 2013. Multi-analytical pedosystem approach to characterizing and interpreting the fossil record of soils. In: Driese, S.G., Nordt, L.C. (Eds.), New Frontiers in Paleopedology and Terrestrial Paleoclimatology SEPM Special Publication 104, pp. 89–107.

Oliver, J.S., 1994. Estimates of hominid and carnivore involvement in the FLK *Zinjanthropus* fossil assemblage: some socioecological implications. Journal of Human Evolution 27, 267–294.

Plummer, T.W., Bishop, L.C., 1994. Hominid paleoecology at Olduvai Gorge, Tanzania as indicated by antelope remains. Journal of Human Evolution 27, 47–75.

Potts, R., 1982. Lower Pleistocene Site Formation and Hominid Activities at Olduvai Gorge. Harvard University, Cambridge, MA, Tanzania (494 pp.).

Potts, R., 1984. Home bases and early hominids. American Scientist 72, 338–347.

Potts, R., 1988. Early Hominid Activities at Olduvai. Aldine de Gruyter, Hawthorne, NY.

Retallack, G.J., 1988. Field recognition of paleosols. In: Reinhardt, J., Sigleo, W.R. (Eds.), Paleosols and Weathering Through Geologic Time. Geological Society of America, Special Paper 216, pp. 1–20.

Retallack, G.J., 2001. Soils of the Past: An Introduction to Paleopedology (2nd edition). Blackwell Science, Ltd., Oxford (416 pp.).

Schoeneberger, P.J., Wysocki, D.A., Benham, E.C., Soil Survey Staff, 2012. Field book for describing and sampling soils, version 3.0. Natural Resources Conservation Service. National Soil Survey Center, Lincoln, NE.

Sheldon, N.D., Tabor, N.J., 2009. Quantitative paleoenvironmental and paleoclimatic reconstruction using paleosols. Earth Science Reviews 95, 1–52.

Sheldon, N.D., Retallack, G.J., Tanaka, S., 2002. Geochemical climofunctions from North American soils and application to paleosols across the Eocene–Oligocene boundary in Oregon. Journal of Geology 110, 687–696.

Sikes, N.E., 1994. Early hominid habitat preferences in East Africa: paleosol carbon isotopic evidence. Journal of Human Evolution 27, 23–45.

Soil Survey Staff, 2014. Illustrated Guide to Soil Taxonomy. U.S. Department of Agriculture, Natural Resources Conservation Service, National Soil Survey Center, Lincoln, Nebraska (552 pp.).

Southard, R.J., Driese, S.G., Nordt, L.C., 2011. Vertisols. In: Huang, P.M., Li, Y., Sumner, M.E. (Eds.), Handbook of Soil Science, 2nd Edition CRC Press, Boca Raton, Florida (Chapter 33.7, p. 33–82 to 33–97).

Stoops, G., 2003. Guidelines for Analysis and Description of Soil and Regolith Thin Sections. Soil Science Society of America, Madison, WI (184 pp. + CD w/images).

Survey Staff, Soil, 2004. Soil Survey Laboratory Methods Manual. U.S. Department of Agriculture, Natural Resources Conservation Service, National Soil Survey Center, Lincoln, Nebraska. Soil Survey Investigations Report 42 (700 pp.).

Tobias, P.V., 1967. Olduvai Gorge, Volume 2: The Cranium and Maxillary Dentition of *Australopithecus* (*Zinjanthropus*) *boisei*. Cambridge University Press.

Turk, J.K., Chadwick, O.A., Graham, R.C., 2011. Pedogenic processes. In: Huang, P.M., Li, Y., Sumner, M.E., Huang, P.M., Li, Y., Sumner, M.E. (Eds.), Handbook of Soil Science, 2nd Edition CRC Press, Boca Raton, Florida (Chapter 30, p. 30–1 to 30–29).

Uribelarrea, D., Domínguez-Rodrigo, M., Pérez-González, A., Vegas Salamanca, J., Baquedano, E., Mabulla, A., Musiba, C., Barboni, D., Cobo-Sáchez, L., 2014. Geo-archaeological and geometrically corrected reconstruction of the 1.84 Ma FLK Zinj paleolandscape at Olduvai Gorge, Tanzania. Quaternary International 322–323, 7–31.

van der Merwe, J.N., Masao, F.T., Bamford, M.K., 2008. Isotopic evidence for contrasting diets of early hominins *Homo habilis* and *Australopithecus boisei* of Tanzania. South African Journal of Science 104, 153–155.

Vepraskas, M.J., 1996. Redoximorphic features for identifying aquic conditions. Raleigh, NC Agricultural Experiment Station. Technical Bulletin 30 (33 pp.).

Vepraskas, M.J., Faulkner, S.P., 2001. Morphological features of seasonally reduced soils. In: Richardson, J.L., Vepraskas, M.J. (Eds.), Wetland Soils: Genesis, Hydrology. Landscapes and Classification. Lewis Publishers, New York, pp. 163–182.

Wilding, L.P., Tessier, D., 1988. Genesis of Vertisols: shrink–swell phenomena. In: Wilding, L.P., Puentes, R. (Eds.), Vertisols: Their Distribution, Properties, Classification and Management. Texas A&M University Printing Center, College Station, pp. 55–81.

Winchester, J.A., Floyd, P.A., 1977. Geochemical discrimination of different magma series and their differentiation products using immobile elements. Chemical Geology 20, 325–343.

Please cite this article as: Driese, S.G., Ashley, G.M., Paleoenvironmental reconstruction of a paleosol catena, the Zinj archeological level, Olduvai Gorge, Tanzania, Quaternary Research (2015), http://dx.doi.org/10.1016/j.yqres.2015.10.007